Design, Modeling and Analysis of a New Power Swing Protection Scheme for Wind Integrated Systems

A Thesis

Presented in Partial Fulfillment of the Requirements for the

Degree of Master of Science

with a

Major in Electrical Engineering

in the

College of Graduate Studies

University of Idaho

by

Maadhavi Sathu

Major Professor: Yacine Chakhchoukh, Ph.D.

Co-Major Professor: Brian K. Johnson, Ph.D.

Committee Members: Joseph D. Law, Ph.D.; Hangtian Lei, Ph.D.

Department Administrator: Joseph D. Law, Ph.D.

December 2020

Authorization to Submit Thesis

This thesis of Maadhavi Sathu, submitted for the degree of Master of Science with a major in Electrical Engineering and titled "Design, Modeling and Analysis of a New Power Swing Protection Scheme for Wind Integrated Systems," has been reviewed in final form. Permission, as indicated by the signatures and dates below, is now granted to submit final copies to the College of Graduate Studies for approval.

Major Professor: _____ Date: _____

Yacine Chakhchoukh

Co- Major Professor: _____ Date: _____

Brian K. Johnson

Committee Members: _____ Date: _____

Joseph D. Law

_____ Date: _____

Hangtian Lei

Department Administrator: _____ Date: _____

Joseph D. Law

Abstract

An increasing number of wind farms acting as power plants are connected directly to power transmission networks, supplanting conventional synchronous machine-based generation. The effect of these wind generators on the dynamic performance of the power system is becoming increasingly important as power swing rates increase with decreased system inertia. In this thesis, power swing blocking protection element operation is analyzed in context of large-scale penetration of Type 4 grid integrated wind turbine systems. The underlying converter controls for large Type 4 WTG plants are designed and integrated to 12-bus benchmark power system modeled using a Real Time Digital Simulator (RTDS). The dynamic response characteristics of the integrated wind generation systems are compared against synchronous generators during fault-contingencies by utilizing a distance protective relay model in RTDS to analyze the effective impedance seen by the relay during a power swing. Differences in the operation of the distance protection element are studied and an improved protection element is designed to ensure correct operation of the relays. The results for fault contingencies with WTG's demonstrated the effectiveness of the protection scheme.

Acknowledgments

I thank my major advisor Dr. Yacine Chakhchoukh, for all his guidance and support throughout my research and Master's program.

Also, I extend my gratitude to Dr. Brian Johnson for his insightful ideas and support throughout my journey.

I'm thankful to Dr. Hangtian Lei and Dr. Joseph D. Law for their time and patience to evaluate my work and thesis and for their valuable suggestions.

This is also the perfect opportunity to thank Mr. John Jacksha for his assistance during my study and the staff of ECE department who have been a part of the completion of my Master's Degree.

Table of Contents

List of Figures

List of Tables

Acronyms

RTDS - Real Time Digital Simulator

ROCOF - Rate of Change of Frequency

OOS - Out of Step

PSB - Power Swing Blocking

OST - Out of Step Tripping

SCV - Swing Center Voltage

OSB - Out of step Blocking

PSS/E - Power System Simulator for Engineering

CT - Current Transformer

VT - Voltage Transformer

CVT- Capacitive Voltage Transformer

BCG - B-phase to C-phase to ground fault

RMS - Root Mean Square

WTG - Wind Turbine Generator

VSC - Voltage Source Converter

PSCAD/EMTDC - Power System Computer Aided Design/Electromagnetic Transients including DC

PWM - Pulse Width Modulation

PLL - Phased Locked Loop

PCC - Point of Common Coupling

RSCAD -Real time digital Simulator Computer Aided Design

Chapter 1: Introduction

With the increase in global demand for electricity, the renewable sources of energy such as wind and solar are preferred over conventional coal, gas, nuclear and hydro generation sources. Renewable generation reduces the dependence on fossil fuels and positively impacts air quality and the environment. However, these renewable electricity generation sources behave differently from conventional synchronous rotating machines. Indeed, photovoltaic sources and most wind turbines are connected to the grid through power electronics devices and do not contribute to the system inertia because of the electrical decoupling between generator and grid.

The inertia in the rotating masses of synchronous machines determines the frequency response of the overall system during disturbances which reflects the energy balance. When there is a frequency change in the system, the rotating masses of the synchronous generators will inject or absorb power into or from the grid through their rotational inertia to counteract the frequency deviation [1]. This transfer of energy to or from rotation masses kinetic energy will cause small changes in their rotor speed before being regulated by their governors. The lower the system inertia, the lower the kinetic energy to respond to disturbances, which results in more significant frequency deviations during disturbances.

1.1 Literature Review

With the rapid growth of wind and photovoltaic generation coupled to the AC grid, research is being conducted to verify their impact on system stability and assess the proper and reliable operation of the transmission protection schemes. The system inertia decreases with this standard inverter controls for this type of generation which results in an acceleration of the frequency of the dynamic response of the system to the disturbance. This acceleration can have

big impacts on the stability, control and protection of the grid, which needs to be investigated [1].

Alternate forms of generation such as photovoltaic and wind turbines are connected to the grid through power converters and from the power system point of view, these generation types decoupled from the grid frequency [2]. The overview of system inertia and the impacts on the transmission grid stability is analyzed and the results in [2] indicates that system with lower inertia has higher rate of change of frequency (ROCOF). On the contrary, a system with higher inertia (for example with large amounts of conventional generation in operation) has lower ROCOF. Therefore, it is necessary to provide solutions to assess the impact of this change in system inertia on the response to network events such as loss of generation, loss of load, sudden changes in the demand.

The authors of [3], [5] and [7] discuss the power swing protection settings and its application for the transmission line protection. These approaches differentiate faults, unstable power swings and stable power swings base on the rate of change of effective impedance. To study the behavior of wind generation systems, [10] describes a model of a Type 4 Wind Turbine Generator (WTG) to investigate the performance of transmission line protection with electronically decoupled generation. With the Type 4 wind integrated generation systems, the power swing amplitudes and frequencies (temporary variation of three phase power flow caused by power system disturbances) for the power system increase and may result in the mis-operation of protection relay. In [4], the authors discuss case studies on the mis-operation of power swing protection schemes, characterizing the impacts of factors such as wind generator type, power converter control scheme, wind generation level and capacity. However, there is no mention of power swing protection scheme that works for the wind integrated generation

systems to prevent mis-operation of protective relays. This thesis concentrates on the impact of increased penetration of Type 4 WTG in a system with conventional generation on the system inertia and subsequent impact on power swing blocking protection. A new approach for power swing blocking protection is proposed and tested.

1.2 System Inertia

Synchronous generators are synchronized to the grid in normal operation. The rated kinetic energy associated with a synchronous machine is defined at the nominal frequency (f_{nom}) and is expressed in (1.1) [2].

$$E_{kinetic\_rated} = \frac{1}{2} \cdot J \cdot (2\pi f_{nom})^2 \tag{1.1}$$

Where, J is the total moment of inertia of the rotating mass

f_{nom} is the nominal frequency

The inertia time constant (H) is defined as the kinetic energy of the machine rotor at synchronous speed, in Joules, divided by the Volt-Ampere rating of the generator, and is given in (1.2) [2]. It is a normalized measure of the kinetic energy of the rotor at synchronous speed; and represents the number of seconds the machine can provide rated power with no energy from the prime mover. This normalized measure facilitates per unit analysis of the power system.

$$H = \frac{E_{kinetic}}{S_{rated}} \tag{1.2}$$

Where, H is the Inertia time constant in Joules/VA or per unit seconds

S_{rated} is the three phase voltampere rating of the generator.

The power grid contains many such synchronous rotating machines, each with a certain total inertia. The total system inertia with *i* of synchronous generators is the weighted sum of the individual generating stations and is given in (1.3).

$$H_{sys} = \sum_i \frac{(H_i.S_i)}{S} \tag{1.3}$$

Where *S* is the system MVA base. Equation (1.3) normalizes the *H* values for each machine on the same per unit base. As a result of the weighted sum, the total system inertia is directly proportional to the number of operating synchronous generators in the power system and their individual inertia constants [2].

1.3 Effect of Reduced Inertia on Power Swing

A power swing is the transient variation of three-phase power flow caused by power system disturbances such as faults, line switching, load shedding, or generator disconnection. A power swing is stable if the system attains a new state of equilibrium within the acceptable operating boundaries or unstable if the system losses synchronism [3]. During a power swing, the rotor angle of a given synchronous machine increases or decreases relative to the other generators in the power system, causing the changes in voltages and currents. During a stable power swing the rotor angles exhibit a damping oscillatory response with frequencies up to a few Hertz.

Distance protection elements implemented on transmission lines in the system measure the voltage and current quantities and can misinterpret a power swing as a short circuit fault. In such case, the protection element mis-operates. In line distance protection, such an can occurs when the effective impedance trajectory due to the swing enters an operation zone of line distance relay and stays there for a sufficient time, causing undesired tripping of healthy line, as will be discussed in more detail in Chapter 2. A power swing blocking scheme in a relay

prevents such mis-operations and protects the power operational integrity system. The principal function is to avoid unintentional tripping of power system equipment during a stable power swing. Some relays include elements to detect unstable or out of step conditions to enable a controlled separation of the system at predetermined locations to prevent widespread power outages [3].

A power swing protection scheme implemented in a line distance protection element accomplishes these objectives through Power Swing Blocking (PSB) and out of step tripping (OST) functions. Detailed explanation of these functions are presented in Chapter 2.

Inverter-based resources such as wind generation power plants have fault response characteristics that differ from traditional synchronous machine-based generation. The output of wind generation is controlled using a fast-responding converter control scheme which will be discussed in Chapter 4. Given the impact of inverter-based resources on bulk system protection, the performance of various protection schemes are being analyzed and modified [4]. This thesis is analyzing the performance of PSB and OST schemes in systems with high penetration of wind generation.

1.4 Research Objectives

The objective of this thesis is to study the impacts of large-scale integration of wind generation systems on power swing blocking and out of step tripping protection functions. Because of the electrical decoupling between the wind turbine generator and the grid with commonly used control schemes, the generation system doesn’t contribute inertia to influence power system stability in response disturbances. The power system model used for these studies is simulated and tested in a Real-Time Digital Simulator. An improved protection scheme is proposed, developed and tested.

1.5 Overview of the Thesis

The scope of this thesis is as follows,

1. Understand the different power swing protection schemes used for detecting stable and unstable power swings. These are explained briefly in Chapter 2.
2. Implementing a model of the IEEE 12-bus system with conventional synchronous generators and study the response of PSB and OST elements to faults at different locations. This is presented in Chapter 3.
3. The IEEE 12-bus system is modified with one conventional generation site replaced with an aggregated Type 4 wind generation system with an equivalent real power rating. The wind turbine model and design of control inner and outer control loops, compensator gain calculation and its integration to the 12-bus power system are presented in Chapter 4. The response of PSB and OST elements with the synchronous generation replaced be wind turbines is studied and compared to the results from Chapter 3.
4. The design of a new protection scheme for detecting power swings in systems with high swing frequencies due to high penetration of wind generation is proposed, implemented and tested in Chapter 5.
5. Conclusions and suggestions for future work are discussed in Chapter 6.
6. The test system distance element and the parameters calculations are presented in Appendix A.

Chapter 2: Power Swing Detection Techniques

Power system stability is the ability of an electric power system to attain a new state of operating equilibrium after being subjected to disturbances such as power system faults, significant load shedding, line switching, and loss of large generation units. Certain power system disturbances may result in loss of synchronism between a generator and the rest of the utility system [3]. If such a loss of synchronism occurs, the generator or system areas operating asynchronously must be separated immediately to avoid cascading outages and equipment damage.

2.1 Power System Stability

There is a balance between the mechanical input torque and the output electric torque of each generator during steady-state conditions. Each generator operates near to the nominal frequency and at a constant speed. If there is any system disturbance, this equilibrium is disturbed and leads to the acceleration or deceleration of the rotors of the synchronous machines [5]. If one generator runs faster than the other, the angular position of the rotor relative to the slower machine in the power system will increase. The resulting angular difference transfers part of load from the slow machine to faster machine. This tends to reduce the speed difference and hence the angular separation. After a certain limit, an increase in angular separation is accompanied by a decrease in power transfer. This results in further angular separation that leads to instability caused by the sustained torque imbalance [5].

Small changes in the electrical system configuration causes oscillations in the rotor angle of the generator, and the study of the ability of the power system to maintain stability under these circumstances is known as steady-state stability or small disturbance rotor angle stability analyses. The time frame for these oscillations is in the order of 10 to 20 sec [5]. During nearby

three phase faults, the ability of the power system to transfer power produced by generators is decreased, decreasing the electric power absorbed from generators, whereas the mechanical input to the generators is relatively constant. These type of changes causes severe oscillations in rotor angles of the machines and swings in power flows. The study of the ability of the power system to maintain synchronism between generators under large disturbances, is termed transient stability analysis. The time frame of these damped oscillations is in the order of 3 to 5 sec [5].

2.2 Power Transfer between Two Equivalent Sources

For a transmission line connecting two equivalent generators shown in Figure 2.1, the active power *P* transferred between two generators is given in equation (2.1), with the assumption the resistances are negligible.

$$P = \frac{E_S . E_R}{X} \cdot \sin \delta \tag{2.1}$$

Where, E_s is the sending end source voltage magnitude

E_R is the receiving end source voltage magnitude

δ is the angle difference between the two sources

X is the total reactance between two generators given in equation in (2.2)

$$X = X_s + X_L + X_R \tag{2.2}$$

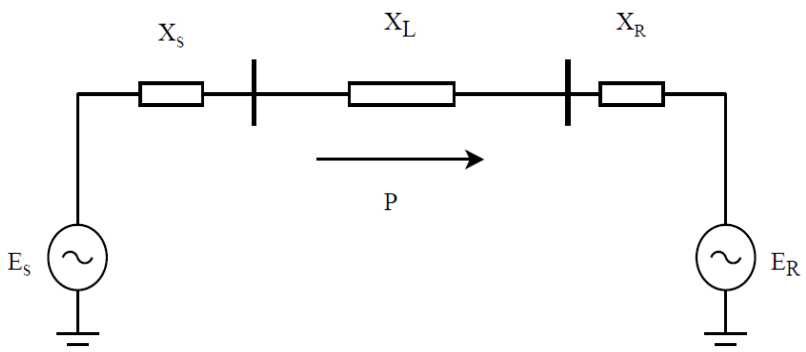

Figure 2.1: A Two Source System

2.2.1 Power Angle Curve

With constant E_S, E_R and X values, the relation between P and δ is represented in a Power Angle curve, shown in Figure 2.2. The real power transferred between two generators is zero for $\delta = 0$ and increases with an increase in δ. The maximum power transferred between two sources is attained at $\delta = 90$ degrees, and a further increase in δ will result in a decrease of the power transfer.

During steady-state operating conditions, the mechanical input power P_0 is converted into an equivalent amount of electric power and transferred over the lossless transmission line. The angle difference angle at this operating point is δ_0 as shown in Figure 2.2.

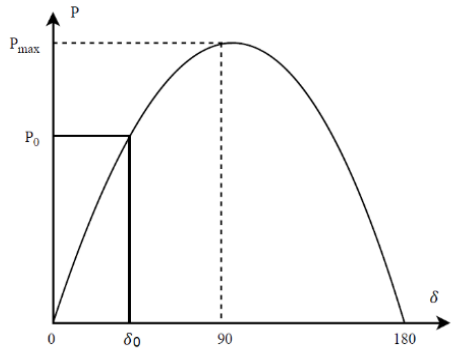

Figure 2.2: The Power Angle Curve [5]

2.3 Equal Area Criteria

The two-source power system shown in Figure 2.1 is operating at a balance point δ_0, with total power transfer P_0. When a three-phase fault with fault resistance occurs on the transmission line, the electric power output is reduced to P_F, the generator rotor starts to accelerate since $P_a = P_0 - P_F$, and δ starts to increase. After some time, the fault is cleared, and at that instance, the angle difference between the two sources is δ_C, and the power transfer is P_C. There is a decelerating torque acting on the rotor because the electric power P_C is higher than the mechanical input power P_0. Due to the gain in kinetic energy in the inertia of the machine, the angle does not stop increasing and go back to δ_0 immediately, and instead continues to increase to δ_F. The energy that must be lost during the deceleration in area 2 is equal to the energy gained during the acceleration in area 1. This description of this behavior is called the equal area criterion.

The system is transiently stable if δ_F is smaller than δ_L as shown in Figure 2.3. The angle difference between the two sources returns to the original point δ_0 with sufficient damping.

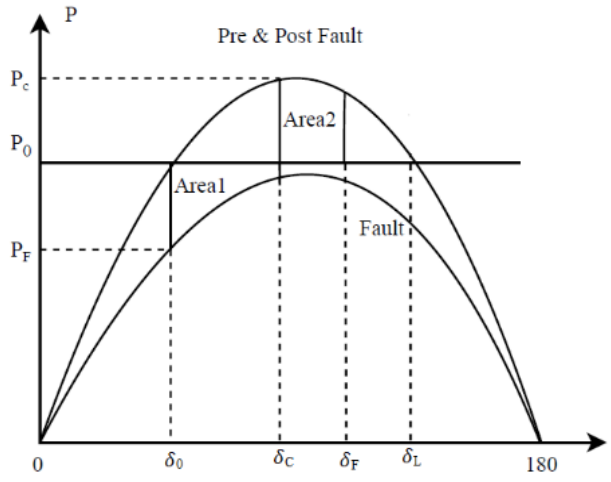

Figure 2.3: A Transiently Stable System Response to a Fault [5]

If area 2 is smaller than area 1 at the time when the angle reaches δ_L, then any further increase in angle results in the electric power output smaller than the mechanical input. Therefore, the rotor will continue to accelerate rather than decelerating. This type of scenario is called a transiently unstable system and the two areas are shown in Figure 2.4. When an unstable condition exists in the power system, one equivalent generator rotates at a different speed from the other equivalent generator, such type of event is called a Loss of Synchronism or Out of Step condition.

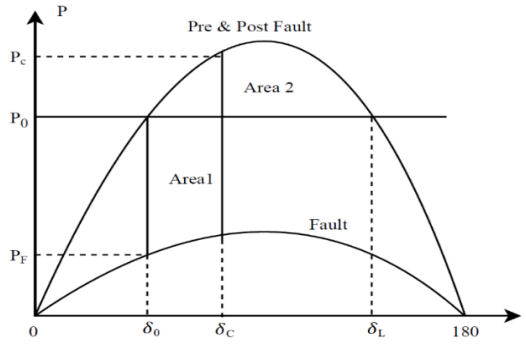

Figure 2.4: Static Characteristics for a Transiently Unstable System [5]

2.4 Representation of Power Swing in the Impedance plane

The network used to study the power swing phenomenon is the single-machine, infinite bus model given in Figure 2.5 [3]. The voltage source E_S has an phase angle theta that is positive relative to the remote source, and it will vary during the power swing. The source E_R represents an infinite bus, and the angle will not vary with time.

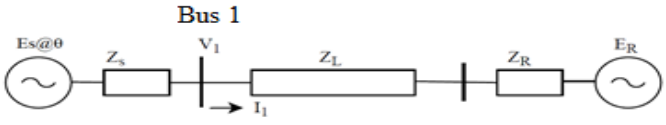

Figure 2.5: Two Sources Equivalent Elementary Network [5]

The effective positive sequence impedance Z_1 phasor calculated at Bus 1 is provided by equation (2.3).

$$Z_1 = \frac{V_1}{I_1} \tag{2.3}$$

Assuming the two sources have equal voltage magnitudes, the impedance trajectory in the complex plane as θ varies with time due to a power swing is given in (2.4).

$$Z_1 = \frac{Z_T}{2} \times \left(1 - j \cdot \cot\frac{\theta}{2}\right) - Z_s \tag{2.4}$$

Where, Z_T is the total positive sequence impedance between two sources E_s and E_R and Z_s is the source positive sequence impedance of source E_s

The locus of the effective Z_1 impedance phasor is the straight line that intersects the line segment Z_T perpendicularly at its center point, as shown in the Figure 2.6. The intersection occurs when the angle difference between two sources is 180 degrees, and the point of intersection if the electrical swing center for the system [3].

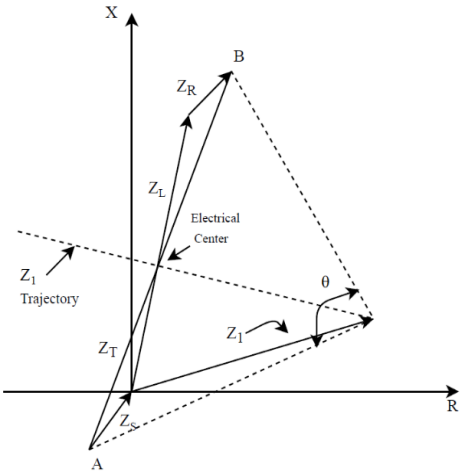

Figure 2.6: Locus of Effective Z_1 Impedance Phasor During a Power Swing with Sources of Equal Voltage Magnitudes [3]

In reality, the one of the power sources is not ideal voltage source; it is an effective equivalent of multiple synchronous generators. During a power swing, the ratio of power source magnitudes does not remain constant, and the Z_1 impedance trajectory is not the as simple as described in Figure 2.6. To illustrate this case, let n be the ratio of the unequal magnitudes, which is given in equation (2.5); the locus of Z_1 impedance trajectory corresponds to the circles shown in Figure 2.7. The ratio of two linesegments joining the extremity of Z_1 (P) to the total impedance Z_T extremities A(PA) and B(PB) is equal to the ratio of source magnitudes as shown in equation (2.5).

$$\mathrm{n} = \frac{E_S}{\mathrm{Z_R}} = \frac{\mathrm{PA}}{\mathrm{PB}} \tag{2.5}$$

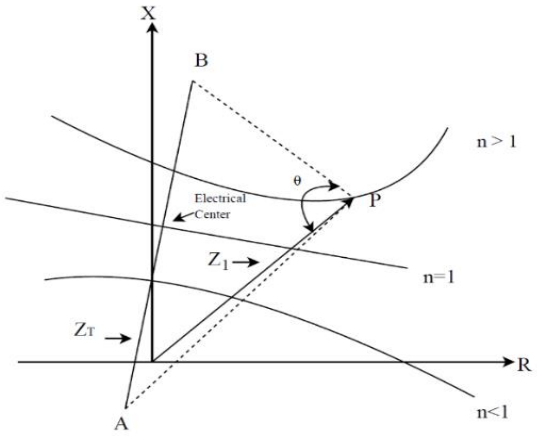

Figure 2.7: Locus of Effective Z_1 Impedance during a Power Swing with Sources of Unequal Volage Magnitudes [3]

2.5 Rate of Change of Positive Sequence Impedance

Assuming the two voltage sources are equal in magnitude, the time derivative of the effective impedance Z_1 is given by equation (2.5).

$$\frac{dZ_1}{dt} = -jZ_T \cdot \frac{e^{j\theta}}{(1-e^{j\theta})} \cdot \frac{d\theta}{dt} \tag{2.5}$$

Assuming the phase angle (θ) has a sinusoidal variation with a slip frequency relative the grid frequency in radians per second given by equation (2.6).

$$\frac{d\theta}{dt} = \omega \tag{2.6}$$

We can determine that $\left|1 - e^{-j*\theta}\right| = 2 * \sin\frac{\theta}{2}$ and the rate of change of Z_1 impedance is expressed as (2.7)

$$\left|\frac{dZ_1}{dt}\right| = \frac{|Z_T|}{4sin^2\frac{\theta}{2}} . |\omega| \tag{2.7}$$

Equation (2.7) expresses the rate of change of the Z_1 impedance which depends on the slip frequency (difference between the grid frequency corresponding and the rotor frequency), , and transmission line impedance. The response in turn depends upon the type of fault, fault duration.

2.6 The Need for Detecting Power Swings

When the synchronism between the power system and generator is not lost, different transmission line relays are affected in different ways. Line differential relay systems do not respond to the out of step condition, but other line protection elements such as overcurrent, directional overcurrent, and distance relays respond to the change of voltage and current, and their phase angle relationship. As a result, they may misoperate for stable power swings due falsely identifying them as faults.

The distance relay could during a power swing if the swing trajectory enters into the relay operating characteristics which is shown in Figure 2.8. The figure shows a $Zone_1$ mho characteristic for a distance relay, which is typically set to trip with no intentional time delay

and is prone to operate during a stable power swing. Backup elements, such as $Zone_2$ or $Zone_3$ elements can also misoperate during stable power swings since the locus of the impedance can stay in the mho circuit until the time delay expires.

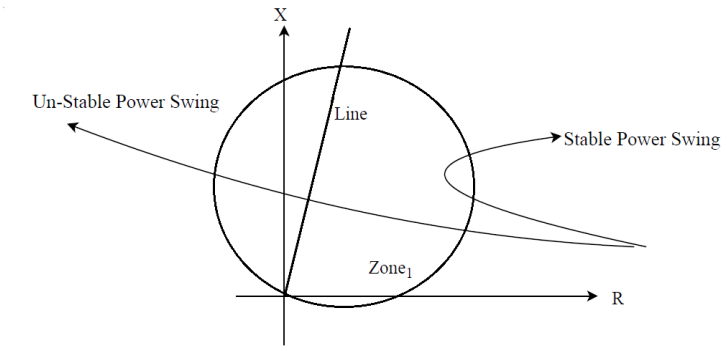

Figure 2.8: $Zone_1$ Characteristics of Distance Element with Stable and Unstable Power Swing Trajectories

To avoid the tripping of any protective element during a stable power swing, while also protecting the power system during fault condition, a power swing blocking (PSB) signal is needed. Moreover, in the case of an unstable power swing, Out of Step Tripping (OST) signal is needed for network separation in order to avoid cascading outages.

2.7 Power Swing Detection Techniques

The traditional detection schemes used for PSB and OST are based on the rate of change of impedance, and newer methods have been developed for use in microprocessor relays [cite ref]. Different methods that are used in power systems for detecting stable and unstable swings are discussed below.

2.7.1 Conventional Rate of Change of Impedance PSB and OST methods

A short circuit fault is an electromagnetic transient process that has a short time constant. The change in the impedance from the pre-fault value to the fault value is short, a few milliseconds and relays are designed to respond quickly. On the other hand, a power swing is an electromechanical transient process with a time constant significantly longer than that of afault. For example, if the frequency of the electromechanical oscillation is about 1 Hz, then the apparent impedance change will have a period on that order. During normal operating conditions, the positive sequence impedance measured by the relay is the load impedance and is well outside of the operating zone of the distance relay. During faults and some power swings, the impedance measured by the relay enters into the operating zone of the distance relay element.

The difference in the rate of change of the impedance is used in the traditional methods to detect an out of step condition and then block the operation of the distance element before the impedance enters into the operating zones of the protective relay. This is accomplished by placing two concentric characteristics separated by impedance ΔZ on the complex impedance plane and a timer to calculate the time taken by the locus of the impedance to travel between them. If the timer does not expire before the measured impedance crosses the concentric characteristics, then the PSB element declares it as a fault. If the timer expires before the measured impedance crosses both the impedance characteristics, then the PSB element declares the event to be a power swing and blocks the distance relay element operation.

Different shapes like concentric polygons, concentric mho, concentric quadrilaterals, as shown in Figure 2.9, have been used in practice for impedance measurement for PSB elements.

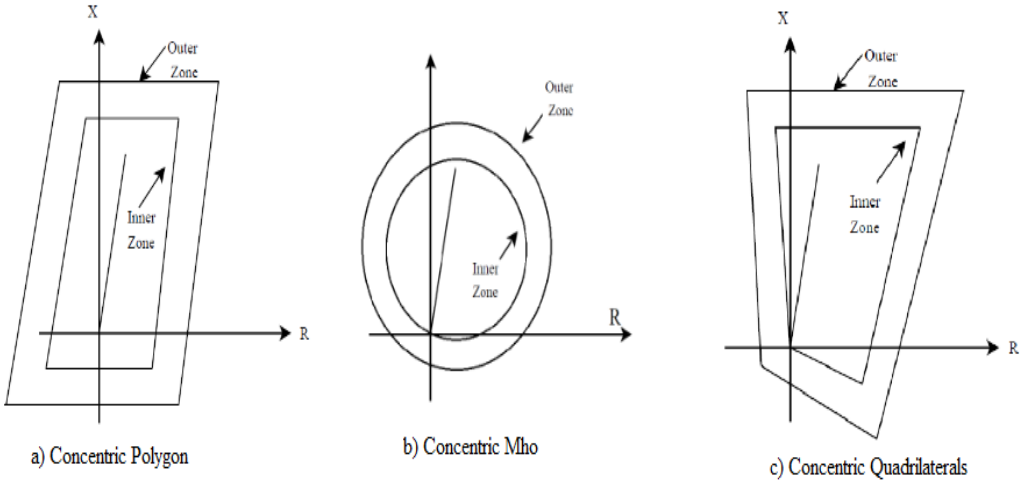

Figure 2.9: Power Swing Blocking and Out of Step Tripping Concentric Distance Relay Characteristics [3]

A single blinder scheme is shown in Figure 2.10. This type of scheme detects an OOS condition when the time required to cross betweem the two blinders exceeds a minimum time setting. The OST signal can be set on the way out of the zone but cannot be implemented for PSB function because the impedance locus enters the $Zone_1$ before the power swing is detected.

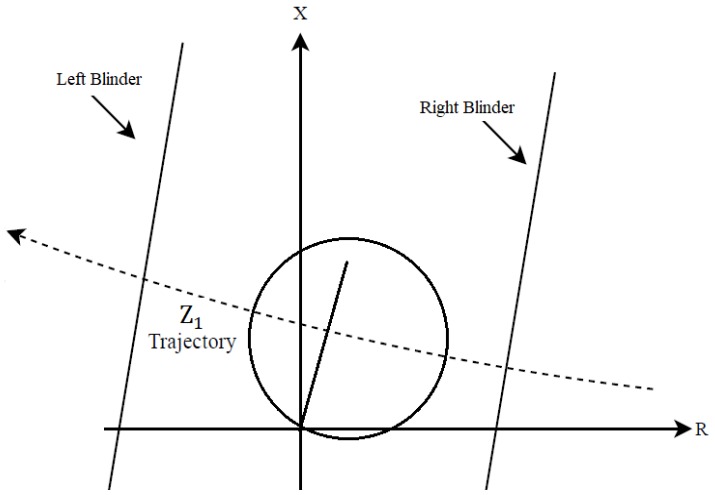

Figure 2.10: Single Blinder OST Scheme

A two blinder scheme is shown in Figure 2.11. During a power swing event, the time taken by the Z_1 impedance trajectory to cross the distance between the outer blinder and the inner blinder is measured. If the measured impedance stays between the outer and inner blinders for a predetermined time, then the event is declared as a stable power swing and an output blocks the distance relay element operation. OST scheme is set to function when the Z_1 impedance enters the way in of the left side inner blinder or on the way out of the Zone charctersictics of the distance relay.

This method for detecting power swings is implemented in this thesis in the test system for studying the performance of the distance element with integration of wind generation.

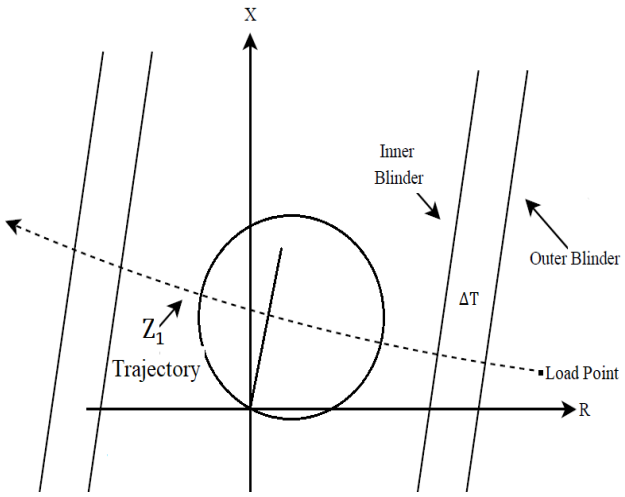

Figure 2.11: Two Blinder Scheme

2.7.2 Non-Conventional Power Swing Detection Methods

2.7.2.1 Rate of Change of Swing Center Voltage

The Swing Center Voltage (SCV) is defined as the voltage at the location n the equivalent power system where the voltage magnitude is zero when the angle between the two sources is 180 degrees apart during a power swing where effective Z1 crosses bewteen the sources as

shown in Figure 2.5 and 2.6 [6]. A more detailed voltage phasor diagram for a two-source system is shown in Figure 2.12.

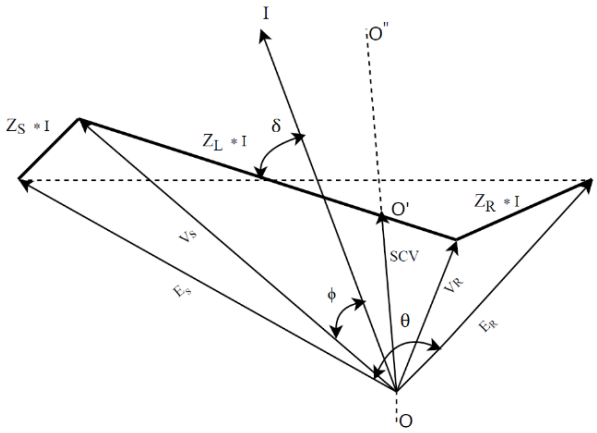

Figure 2.12: Voltage Phasor Diagram of the Two Source System Showing Swing Center Voltage [6]

When the two source equivalent power system experiences a power swing and enters into an OOS condition, the angle difference between the two sources, $\theta(t)$, increases as a function of time and is given in equation (2.8). Assuming the two sources have equal magnitudes, E, *SCV*(t) is the instantaneous voltage at the swing center. An estimated SCV that the relay calculates will be discussed later.

$$SCV(t) = \sqrt{2}\mathrm{E}\sin\left(\omega t + \frac{\theta(t)}{2}\right) \cdot \cos\frac{\theta(t)}{2} \tag{2.8}$$

The equation is a typical amplitude modulated sinusoidal waveform, where the first sine term is the base sinusoidal wave, or the carrier, with an average frequency of $\omega t + \frac{\theta(t)}{2}$. Furthermore, the second term is the cosine amplitude modulation[6].

Figure 2.13, shows the positive sequence SCV with an average frequency of 50 Hz [6] and a constant slip frequency of 5 Hz during a system OOS condition. The magnitude of the swing

center voltage fluctuates between zero and one per unit of the system nominal voltage, and the magnitude of the voltage is forced to zero every 0.2 sec due to the slip frequency of 5 Hz. Under normal load conditions, the RMS magnitude of the SCV is constant.

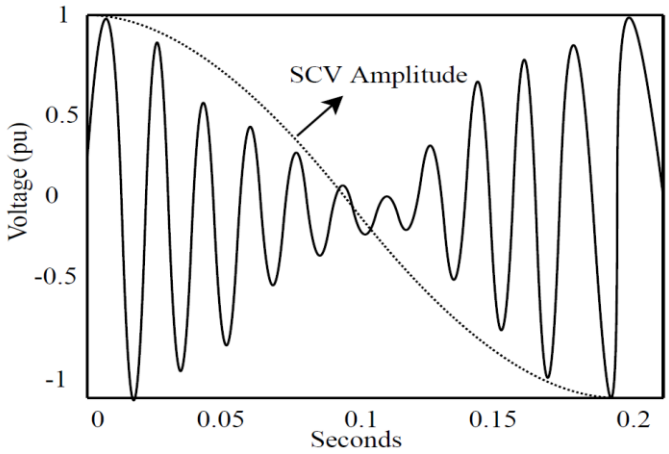

Figure 2.13: Swing Center Voltage During an OOS Condition

2.7.2.2 SCV Local Estimate

Generally it is not possible to directly measure the swing center voltage since it is not at a substation. In addition, the swing center can vary as system topology changes. Instead, relays can estimate the SCV using the locally available quantities. One popular estimate of the SCV is given in equation (2.9).

$$SCV \approx |V_s| \cos \phi \tag{2.9}$$

Where $|V_s|$ is the magnitude of the locally measured voltage at Bus 1 in Figure 2.5 and ϕ is the angle difference between the local current and voltage.

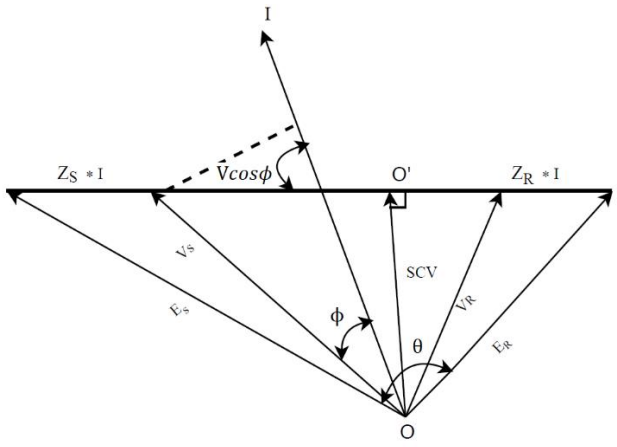

Figure 2.14: $V_s \cos\phi$ is a Projection of Local Voltage, $V_{s,}$ onto Local Current I.

As shown in Figure 2.14, $|V_s| \cos\phi$ is the projection of V_s on to the current axis, I, which was first introduced by Ilar for detecting power swings [7]. For a homogeneous system with the system impedance angle close to 90 degrees, $|V_s| \cos\phi$ is a well-approximated value for the swing center voltage. For detection of power swings using this method, the rate of change of SCV provides the primary information of system swings. As a result, some difference in magnitude between the system SCV and the local estimate has little impact in detecting power swings since the error due to the approximation doesn't have much impact on the rate of change.

By keeping in mind that the local SCV estimation is made using the magnitude of the local voltage, the relation between the SCV and the phase angle difference, θ, of the two source voltage phasors can be obtained by simplifying equation (2.8) to the following equation (2.10)

$$SCV_1 = E_1 \cos\left(\frac{\theta}{2}\right) \tag{2.10}$$

Where E_1 is the magnitude of the positive sequence source voltage, which is equal to E_S also assumed to be equal to E_R. SCV_1 represents that the positive sequence swing center voltage is used in detecting power swings. This choice is due to the smooth magnitude of SCV_1 during

the OOS condition in the power system. The value of SCV is maximum when the angle between the two sources is zero, and the value is minimum when the angle is 180 degrees. This property has been utilized so that a power swing is identified by calculating the rate of change of SCV.

The derivative of the SCV_1 is given by equation (2.11):

$$\frac{d(SCV_1)}{dt} = -\frac{E_1}{2}\sin\left(\frac{\theta}{2}\right)\frac{d\theta}{dt} \tag{2.11}$$

The relation between the rate of change of SCV and the rate of change of the two machine system slip frequency $(\frac{d\theta}{dt})$ is provided by equation (2.11). It is observed that the derivative is independent of the power system impedances. A plot of the SCV and the rate of change of SCV for a system with a constant slip frequency of one radian per second is shown in Figure 2.15.

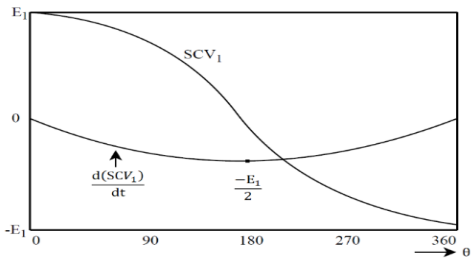

Figure 2.15: SCV_1 and its Rate of Change with Unity Source Voltage Magnitudes

2.7.2.3 Continuous Impedance Calculation

This method determines a power swing condition based on a continuous effective impedance calculation [3]. The impedance is calculated and compared against the the value from the previous over a running 5 ms time step. If there is a deviation, an OOS condition is assumed but not proven. If a change is detected, the algortihm predicts a value for the next impedance value that should be calculated 5 ms later based on the change in impedance relative to the previous step. If the prediction is correct, then the power swing condition is detected. The main

advantage of this method when compared to the conventional rate of change of impedance method or rate of change of swing center voltage is that it doen't require any system impedance based settings.

2.7.2.4 Continuous Calculation of Incremental Current

The phase currents and voltages undergo magnitude variationsfollowing a major system disturbance such as severe faults or loss of a major generator. The continuous calculation of the incremental current computes the difference between the present sample value of the current and the value stored in a buffer 2 cycles earlier. When the absolute value of calculated incremental value exceeds five percent of the nominal current for a continuous duration of 3 cycles, then this condition is declared as a power swing.

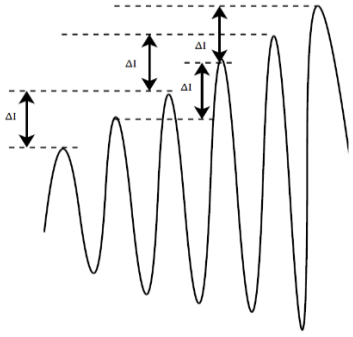

Figure 2.16: Continous Calculation of Incremental ΔI.

2.8 Quantities used for Power Swing Detection

As discussed in the previous section, different quantities are used in the detection of power swings and the implementation of PSB and OST signals. Most conventional relays use the rate of change of impedance measurement method and measure voltage and current at the relay. Other quantities have also been used in PSB and OST elements, such as phase angle difference

across the transmission line and its rate of change, the swing center voltage, and the first derivative of the swing center voltage [5].

2.8.1 Out Of Step Protection Scheme

Traditional ways to minimize the spread of a cascading outage caused by the loss of synchronism is the application of the Out of Step (OOS) protection scheme. It detects the OOS condition and takes necessary actions to remove the affected area, minimize the loss of load and maintain service continuity. The essential function of the out of step tripping scheme is to differentiate between unstable and stable power swings and execute network separation or island the system during the loss of synchronism. An Power Swing Blocking (PSB) scheme differentiates between faults, stable power swing and blocks relay element prone to operate during stable swings. This scheme must also allow the relay to operate during faults or faults that evolve during an out of step condition.

Chapter 3: System Design

This chapter focuses on the implementation of the IEEE 12-bus system for studying the effects of the integration of wind generation. The distance protection element is designed to simulate the response of the PSB and OST functions under various system faults. A Real-Time Digital Simulator (RTDS) is used for these system studies, and the following sections give a brief discussion of the test system.

3.1 The Real-Time Digital Simulator (RTDS)

The RTDS is the real-time simulator used for power system simulations where protection and control hardware can interact with the simulation in real time. RSCAD is a graphical interface package used to develop and run cases on the RTDS. In this work, relays, fault controls and the power system design are developed in RSCAD and are simulated and compiled using the Draft program, and then the Runtime module is used for applying the system disturbances and monitoring the changes in the system.

3.2 IEEE 12-Bus Test System

The IEEE 12-Bus system test model shown in Figure 3.1 was developed at University of Manitoba to support an IEEE working group project. The system is convenient for studying FACTS device applications, transient stability enhancement schemes, and the integration of wind generation [12]. The test system shown in the Figure 3.1 has two 345 kV buses, four 22 kV buses, and six 230 kV buses. The transmission system consists of 230 kV transmission lines except for one 345 kV line linking buses 7 and 8. The generation capacity of generators G2, G3, G4, model data for the lines and transformers, along with shunt capacitances and loads used in this thesis are presented in Table 3.1 and Table 3.2. G2 and G4 are hydro generators and

hence modeled as salient pole machines. G3 is thermal generator and is modeled as round rotor machine. An AC4A type exciter model is used to model the excitation system for all the generators. Mechanical-Hydraulic Controls (GOV1) type model is used for governor control and IEEE hydro turbine model is used for modeling the turbine system. The transformers shown in Figure 3.1 each have a per unit impedances of 0.01 pu with a 100% Tap ratio.

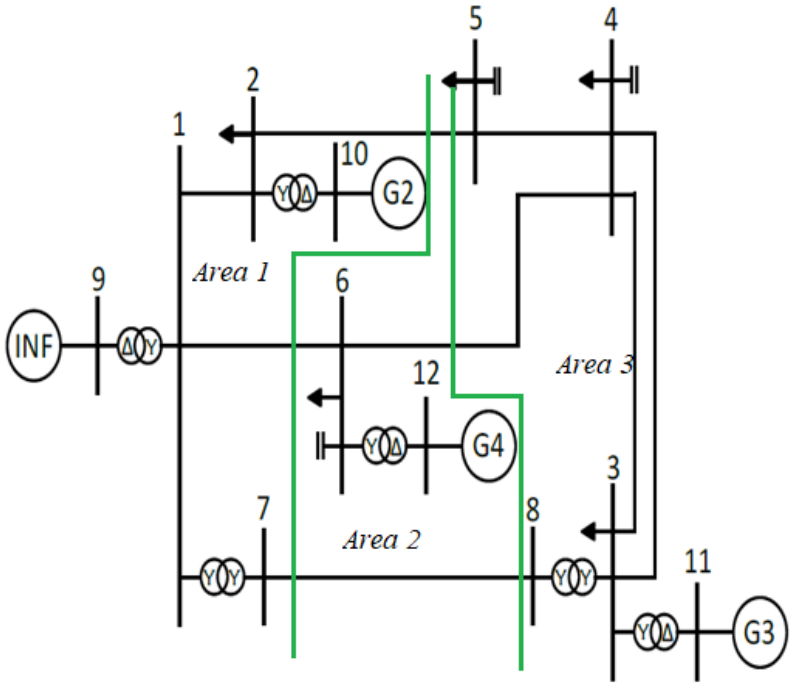

Figure 3.1: One Line diagram of IEEE 12-Bus system [8]

The IEEE 12-bus system is divided in to three main areas based on the overall system oscillation behavior and swing centers (location where the voltage between two sources is zero when angle between two sources is 180 deg during a worst case out of step condition). Area 1 is predominantly a generation area, where the generators connected at Bus 9 and Bus 10 in this region are hydro generators rated 800 MVA and 700 MVA respectively and this area has minimal load. Area 3 in Figure 3.1 is the main load center with some generation available. Generator connected at Bus 11 in this region is a hydro-generator with a 500 MVA rated

machine. Area 2 is the transmission system located between Area 1 and Area 3 with some load and some hydro generation available at Bus12 rated at 500MVA, but this generation is not sufficient to meet the local demand.

Table 3.1: Branch data

From Bus- To Bus	R (pu)	X (pu)	B (pu)
1-2	0.001144	0.09111	0.18261
1-6	0.003356	0.26656	0.55477
2-5	0.03356	0.26656	0.55477
3-4	0.001144	0.09111	0.18261
3-4 (double line)	0.001144	0.09111	0.18261
4-5	0.003356	0.26656	0.55477
4-6	0.003356	0.26656	0.55477
7-8	0.01595	0.17214	3.28530

Table 3.2: Generator, Load and Shunt Capacitor Data

Bus	Type	Gen (MW)	Shunt (MVAr)	Load	
				P (MW)	Q (MVAr)
1	P-Q	-	-	-	-
2	P-Q	-	-	-	-
3	P-Q	-	-	-	-
4	P-Q	-	160	320	240
5	P-Q	-	80	100	60
6	P-Q	-	180	440	300
7	P-Q	-	-	-	-
8	P-Q	-	-	-	-
9	Slack	-	-	-	-
10	P-V	500	-	-	-
11	P-V	200	-	-	-
12	P-V	300	-	-	-

3.3 Steady-State Results Validation

The steady-state power flow results of voltages and angles of the 12-bus system implemented in RTDS are compared with the results obtained from the PSS/E model presented in [8]. Table 3.3 shows the per unit voltage magnitude (pu) and voltage angle (degrees) at each bus and compares the results from RTDS and PSS/E simulation models. The steady-state results for the voltages and angles match very well between the RTDS and PSS/E simulation tools. The results

show that the power flow results from RSCAD is maintained close to the steady-state system condition and can be used for system studies.

Table 3.3: Power flow results at load and generator buses shown in Figure 3.2.

Bus	Voltage (pu)		Angle (degrees)	
	RSCAD	PSSE	RSCAD	PSS/E
1 P-Q	1.0405	1.0405	-2.713	-2.7001
2 P-Q	1.0035	1.0035	-0.8916	-0.8777
3 P-Q	0.9882	0.9881	-38.2630	-38.2737
4 P-Q	0.9561	0.9561	-43.4164	43.4233
5 P-Q	0.9789	0.9789	-30.9564	-30.9454
6 P-Q	0.9893	0.9893	-34.5739	-34.5642
7 P-Q	1.0482	1.0483	-4.4567	-4.43337
8 P-Q	0.9950	0.9949	-36.4376	-36.4500
9- SLACK	1.04	1.04	0	0
10 P-V	1.02	1.02	-28.0915	1.9224
11 P-V	1.01	1.01	-67.1148	-37.1255
12 P-V	1.02	1.02	-61.1651	-31.1555

RSCAD implementation of the system is shown in Figure 3.2

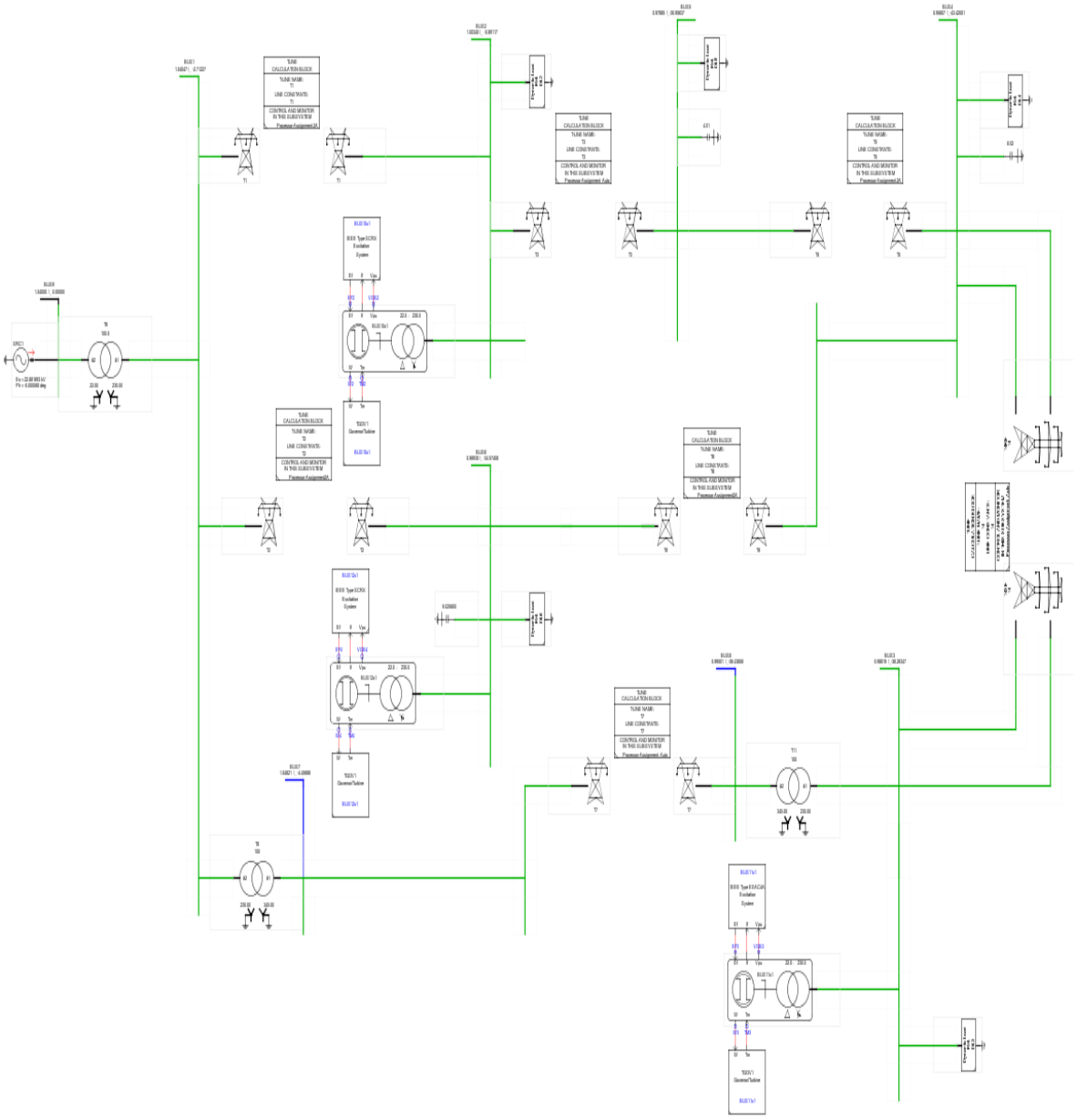

Figure 3.2: IEEE 12 Bus System Power System in RSCAD

The 30-degree angle difference in the voltage angle at buses 10, 11, and 12 is due to the Wye-Delta step up transformers at the generator buses in RSCAD. The simulations in PSSE neglect this transformer phase angle shift.

3.4 System Protection – Basics

The main objective of system protection is to isolate an area in the power system experiencing abnormal operation quickly to reduce outage time and damage caused by the system disturbances. The protective relay measures electrical quantities of the power conductors through Current Transformers (CTs) and Voltage Transformers (VTs) and processes those measurements to detect an abnormal or an intolerable condition when it occurs. These input devices also provide insulation for the relay from high power system voltages and currents. The reduced magnitudes are referred to as secondary levels.

3.5 Current Transformer

The CT is commonly used to step the current down to an appropriate level for a given application. In this study, CT is used to provide input current to protective relays, where the primary current on the main conductors is in kA, and the relay input is the secondary current which is around 5 Amperes for maximum load current. The secondary current is calculated based on the turn's ratio between the primary and the secondary windings.

The secondary current reproduces the primary current over a wide operating range if it is an ideal current transformer. In physical CT, an accurate replica of the primary current in the secondary is possible if the CT operating point is within the linear region shown in Figure 3.3. However, severe conditions, such as when the current rises to many times its steady-state value, the CT operating point could reach the knee point. Beyond this point, the CT goes into saturation and the secondary current measured by the relay is no longer representative of the primary current. A decaying dc offset in the fault current can also drive a CT in saturation.

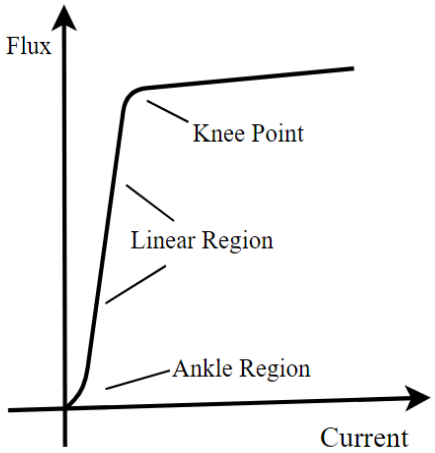

Figure 3.3: Typical CT Magnetizing Characteristic

Current Transformers are usually designed to operate below the knee point even when a high transient current condition occurs. This ensures that the secondary current measured by the relay provides and accurate reproduction of the primary system current condition. When CT saturation does occur, it is often due to decaying dc offsets in the fault currents. The Current transformer implemented in RSCAD for the relay input is shown in Figure 3.4 and the CT parameters for the CTs in Figure 3.4 are listed in Table 3.4.

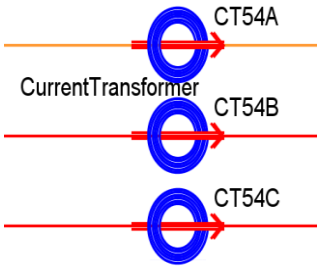

Figure 3.4 CT Representation in RSCAD

Table 3.4: CT Parameters for Transmission Line 5-4

Parameter	Value
Secondary Side Resistance	0.25 ohms
Secondary Side Inductance	0.4 mH
Turns Ratio	500
Burden series Resistance	0.25 ohms
Burden series Inductance	0.1326 mH

3.6 Voltage Transformer

A voltage transformer (VT), also referred to as a potential transformer (PT), is used for measuring voltage on transmission and distribution systems. There are two types of voltage transformers used in protective relaying, wound voltage transformers and capacitive voltage transformers. The operating voltage levels in the power system normally ranges from tens to hundreds of thousands of volts. Relay input voltage levels are generally less than a few hundred volts, therefore a potential transformer is needed to step down the voltage. Very high turns ratios are needed to transmission voltages above 230 kV. To reduce the voltage is stepped down through a capacitive voltage to about 11 kV prior to input to the transformer itself. This is referred to as a capacitive voltage transformer (CVT). CVTs connected line to ground are used in this thesis, as shown in Figure 3.5, with parameters listed in Table 3.5.

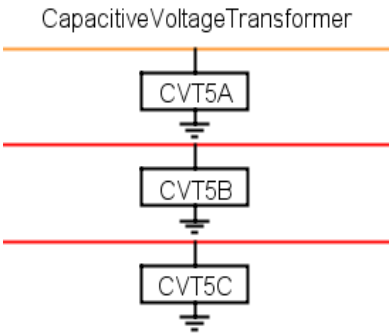

Figure 3.5: CVT Representation in RSCAD

Table 3.5: CVT Parameters for Bus 5

Parameter	Value
Primary Side Resistance	474 ohms
Primary Side Inductance	4.46 H
Primary Side Turns	23000 turns
Secondary Side Resistance	0.18 ohms
Secondary Side Inductance	0.47 mH
Secondary Side Turns	115 turns
Burden Series Resistance	400.9 Ohms
Burden Series Inductance	1.84 H
Burden Parallel Resistance	785 ohms

3.7 System Protection Schemes

The power system is divided into protection areas based on the equipment and the circuit breaker availability. There are six standard areas of protection in the power system:

1. Generator
2. Transformer
3. Bus
4. Line
5. Load (motor, static load)
6. Capacitor or Reactor bank.

These areas have protection relays specially designed for primary protection. The protection is based on the characteristics of the equipment being protected and the protective relays could also be to provide backup for the relays protecting the adjacent equipment. The typical relay primary protection zones in a power system discussed above are shown in Figure 3.6.

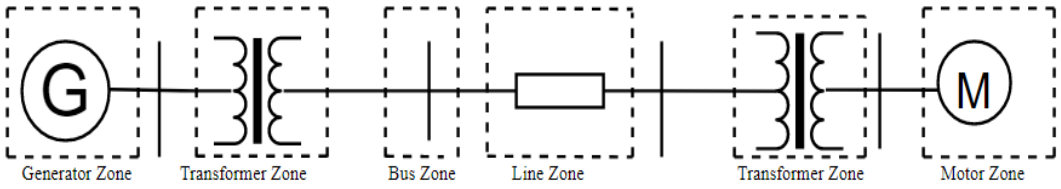

Figure 3.6: Typical Relay Primary Protection Areas in a Power System

The main objective of the system protection is to provide a quick isolation for the area experiencing a problem in the power system. This will permit the rest of the system to stay in service. The five essential features of a system protection are given below [9].

1) Reliability: To ensure that the protection function will operate correctly. It has two aspects, dependability and security. Dependability is the degree of certainty that the relay will function correctly for internal faults, whereas security relates to the degree of certainty that a relay will not operate incorrectly.
2) Selectivity: It is the process of applying and setting of the protective relay such that they operate as fast as possible with in their primary zone but have delayed operation in their backup zone. Operation of the backup protection is incorrect and undesirable unless the primary protection of that area fails to clear the fault with a specific time period. Therefore, selectivity is important to assure maximum service continuity with minimum system disconnection.
3) Speed of Operation: The relay must operate fast enough to detect the faults to prevent equipment damage and system instability.
4) Simplicity: The protection objective should be achieved with minimum protection equipment and associated circuitry.
5) Economics: To ensure maximum protection is achieved at minimal total cost.

The relays acquire their measurements from the power system through CTs and VTs, to system voltages such as 745 kV in North America. Several standard protection schemes are implemented to protect the system from unacceptable power system conditions and to minimize system disruption. Some examples of commonly used protection schemes are overcurrent protection (ANSI/IEEE device number 50), differential protection (87), directional overcurrent protection (32), distance protection (21). This research study focuses on the power swing protection functions used to identify and react to stable and unstable power swings. This function is implemented in the distance protection element (21).

3.8 Distance Protection Scheme

The distance element processes the power system voltage and current obtained from a CT and a CVT and computes an effective impedance which is compared to a threshold. The complex impedance plane or R-X plane is used to analyze distance element operation. The distance element operates when the effective impedance ($\bar{Z}$) given in (3.1) enters the element operating characteristics.

$$\bar{Z} = \frac{\bar{V}}{\bar{I}} \tag{3.1}$$

Where $\bar{V}$ is voltage input signal to the element;

$\bar{I}$ is current input signal to the element.

For normal operating conditions, the measured impedance is effectively a load impedance, $\bar{Z}_{Load}$, due to the of power-flow through the relay, and typically, it is close to the real axis of the R-X plane shown in Figure 3.7. When the fault occurs on the protected line, the measured impedance changes rapidly from $\bar{Z}_{Load}$ to $\bar{Z}_{Fault}$ slowed only by the rate at which the relay processed measurements. With proper input signals to the element, for a bolted fault, $\bar{Z}_{Fault}$ is the positive sequence impedance of the protected line section measured from the relay location to the fault location [3] as shown in Figure 3.7. The distance element typically has one instantaneous zone and two time-delayed zones. Zone 1 and Zone 2 provide primary line protection, and Zone 3 provides the remote back up protection for the adjacent lines.

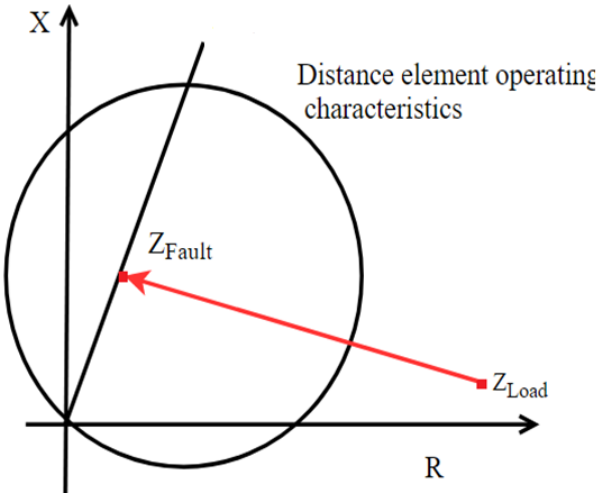

Figure 3.7: Impedance Plane Representation of Distance Element Operation

Typical Zone 1 reach setting for ground elements is 75 percent of the positive sequence line impedance for short lines and up to 90 percent for phase elements for long lines. The Zone 1 reach is set short of the total line impedance to account for errors in the distance element calculation. The time-delayed Zone 2 covers the line section not protected by Zone 1, with some added impedance to account for possible errors. The typical reach setting of Zone 2 is 120 percent of the positive sequence line impedance if the Zone 1 element underreaches by 20 percent of the line impedance [9].

Protecting a three-phase line for different faults requires three phase distance elements and three ground distance elements. A phase distance element responds to three-phase, phase-to-phase and phase-to-ground faults. A ground distance element responds to single-phase-to-ground and phase-to-phase-to-ground faults. The phase and ground distance elements receive information of the faulted phase by measuring the voltage and current and calculating the effective impedance to faulted. For instance, for a BC fault with no fault resistance, the voltage and current are given as $\bar{V} = \overline{V_b} - \bar{V_c}$, $\bar{I} = \bar{I_b} - \bar{I_c}$

$$\bar{Z} = \frac{\bar{V}}{\bar{I}} = mZ_{1L} \tag{3.2}$$

Where Z_{1L} is the line positive sequence impedance.

m is the relay reach, the relative fraction of impedance from the relay location to the fault with respect to Z_{1L} and $\bar{Z}$. The reach is measured in per unit.

For power system faults involving ground, the protective relay doesn't accurately calculate the relative fraction of impedance (m) due to the flow of zero sequence currents and the difference between the positive and zero sequence impedances of the line. To accurately measure the impedance, ground distance element is compensated with a residual current $\bar{I}_r$ shown in (3.3) multiplied by a zero sequence compensation factor, $\bar{k}_0$, given by (3.4).

$$\bar{I}_r = \bar{I}_a + \bar{I}_b + \bar{I}_c \tag{3.3}$$

Where, $\bar{I}_a$ is the measured A phase current

$\bar{I}_b$ is the measured B phase current

$\bar{I}_c$ is the measured C phase current

$$\bar{k}_0 = \frac{\bar{Z}_{0L} - \bar{Z}_{1L}}{3\bar{Z}_{1L}} \tag{3.4}$$

Where, $\bar{Z}_{0L}$ is the line Zero Sequence Impedance.

3.9. Distance Protection in RSCAD for System Studies

The phase voltages and currents are connected to the six inputs of the simulated distance element function. The distance protection element is applied on the line connecting Bus 5 and Bus 4 in the 12-bus system, where the inputs values to the protection relay are obtained from simulated CVTs and CTs. The instantaneous impedance is calculated for the phase-to-phase, phase-to-ground elements. Positive sequence, negative sequence, and zero sequence impedance

quantities are obtained. For detecting phase-to-ground faults, the compensation factor can be calculated automatically in the related model in RSCAD according to equation (3.4) or it can be manually entered as magnitude and angle values.

3.10 Distance element (21)

The distance element used in RSCAD is set with 2 Zones of protection. Zone 1 is set to 70 percent of the line and Zone 2 is a time-delayed element set to 135 percent of the line. Both zones are forward zones. The inputs and outputs for the distance protection relay model used are shown in Figure 3.8.

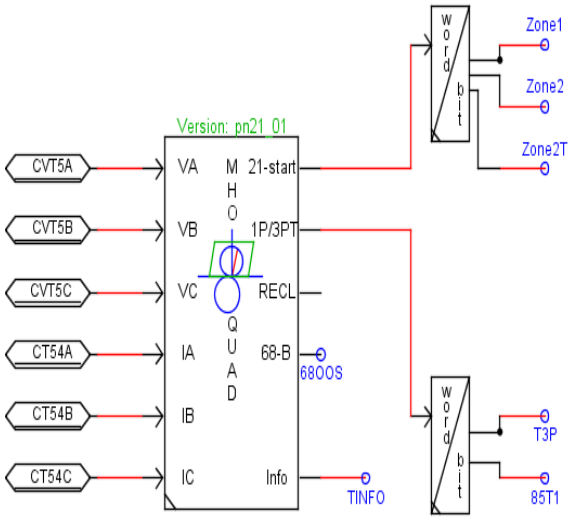

Figure 3.8: Distance Element Implementation in RSCAD

3.11 Out of Step Element (68)

The power swing function uses mho characteristics with a blinder detection scheme employing two concentric mho circles restrained by two sets of parallel blinders. The out of step element (68) is suitable for the supervision of distance element protection and can be used to block or allow tripping during power swings. The blinders set in the distance relay for PSB function are

calculated using Figure 3.9 and the parameters of the used for the settings calculations are given in Table 3.6. The detailed calculation of the values used for setting the distance element (21), Out of Step element (68) are presented in Appendix A.

Table 3.6: PSB Settings Used in Simulation Model

Parameter	**Value**
System Nominal Frequency (f)	60 Hz
Maximum Slip Frequency (s)	5 Hz
Inner Angle	90 degrees
Outer Angle	60 degrees
Transmission Line 5-4 Impedance	Z_{54L}
Equivalent Source Impedance seen at Bus 5	Z_{5s}
Equivalent Source Impedance seen at Bus 4	Z_{5R}
Total Transfer Impedance	$\mathrm{Z_{SecT} = Z_{54L} + Z_{5S} + Z_{5R}}$
Inner Blinder Power Angle δ_1	90^0
Outer Blinder Power Angle δ_2	60^0

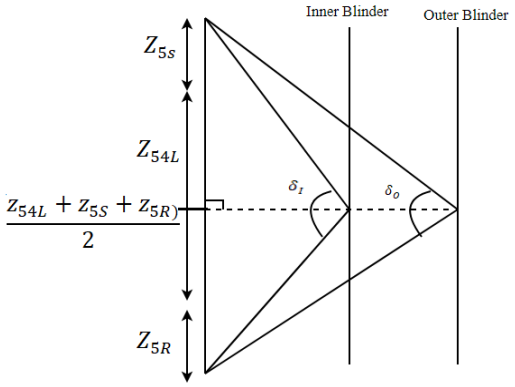

Figure 3.9: Equivalent Source Angles for Setting Power Swing Blinders [6]

Inner Right Resistive Blinder Setting $IR = \frac{|Z_{SecT}|}{2\tan\left(\frac{\delta_1}{2}\right)} = 30$ Ohms (3.5)

Outer Right Resistive Blinder Setting $OR = \frac{|Z_{SecT}|}{2\tan\left(\frac{\delta_2}{2}\right)} = 51$ Ohms (3.6)

Power Swing Blocking Delay (PSBD) $PSBD = \frac{(\delta_1-\delta_2)f}{s\cdot 360^0} = 0.016$ sec (3.7)

A view of the RSCAD diagram showing R-X plane view for studying the operation of distance element showing the zones of distance protection (Zone1, Zone 2) and the two blinder elements discussed above is shown in Figure 3.10. The effective impedance for the steady-state load is shown in the figure. For fault or power swing cases the effective impedance will show as a line showing the trajectory over time.

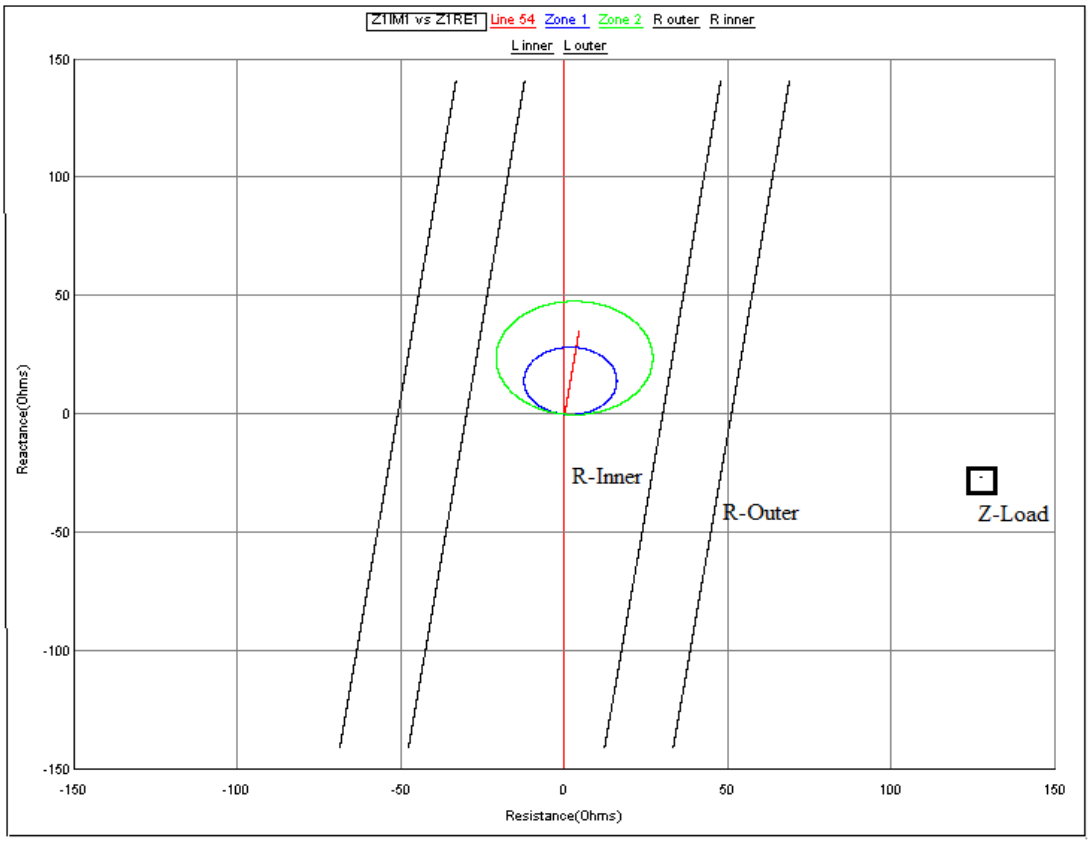

Figure 3.10: Impedance Plot for Power Swing Blocking and Distance Element Protection Response

3.12 Fault Modeling in RSCAD

It is necessary to simulate the behavior of the power system and the protection system to various fault and resulting power swing events. The fault model designed for the test system is shown in Figure 3.11.

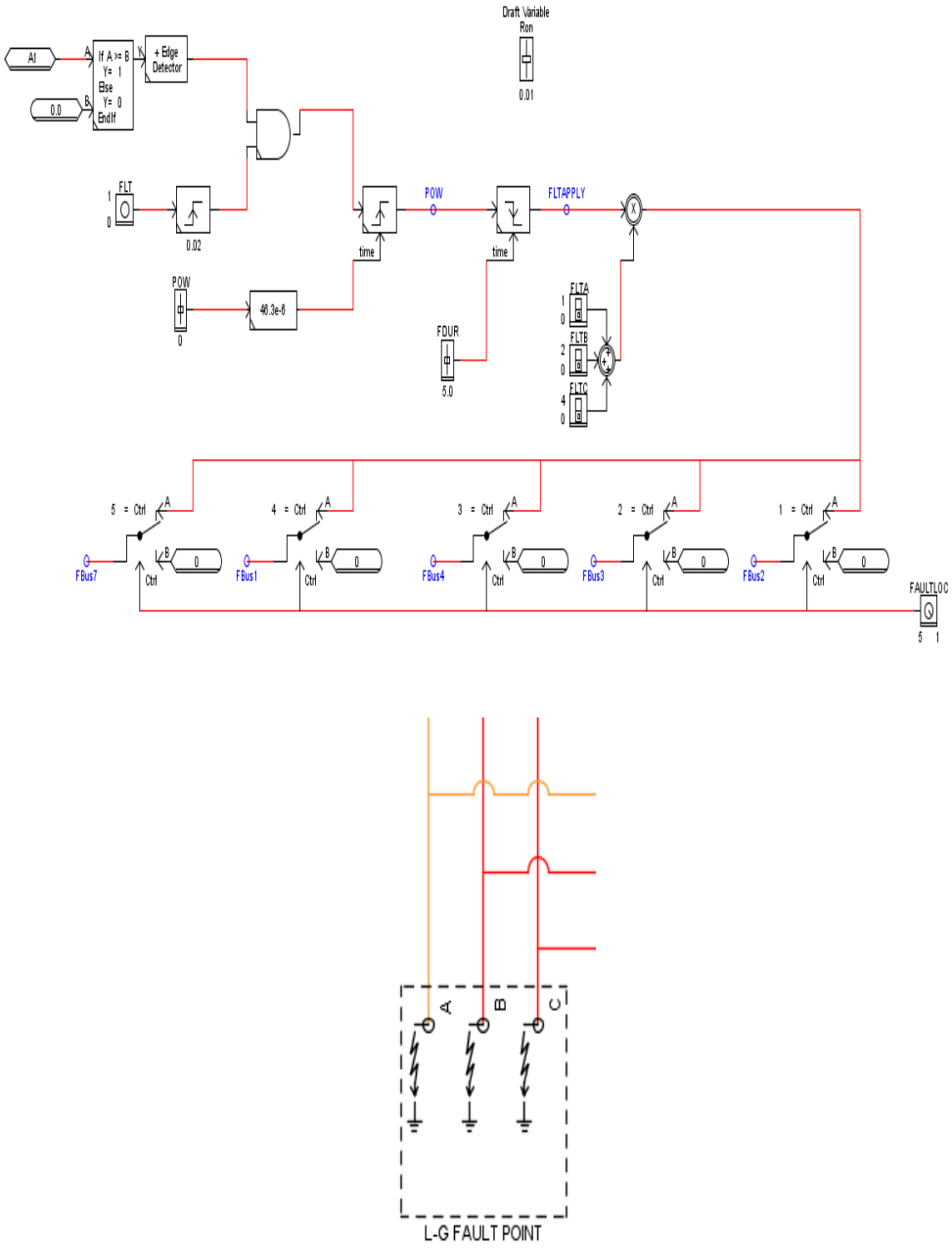

Figure 3.11: The 12-bus Test System Fault Model

The fault model used for the system has specific settings such as Point on Wave (POW) selection, duration of the fault, fault type, fault location, and the fault resistance. The POW function is based on the reference voltage input with a specific time delay to ensure that the fault occurrs at the consistent point on the voltage waveform in repeated studies. The fault type

is selected from the look up table which has bits assigned to particular fault types such as AG, BG, CG. Each fault location has a respective fault number associated with it. Based on the fault number selected, the corresponding fault selector switch asserts, as shown in Figure 3.11, resulting in fault at that specific location.

3.13 Fault Response Simulation cases

Faults are initiated at four different bus locations 3, 4 and 5 in the test system as shown in Figure 3.2. The measured impedance and the response of the distance protection element implemented at the Bus 5 end of Line 5-4 are plotted in each of the fault cases. In each fault case, the fault occurs at t=0.667 s, the fault type is a three-phase fault or a double-line-to-ground fault. The duration of the fault is 0.5 s before the circuit breaker opens to clear the fault.

3.13.1 Case A- Three Phase Fault at Bus 4

A 0.5 s three-phase to ground fault has been applied on Bus 4 resulting in the relay effective impedance trajectory entering into Zone 2 operating characteristics since the fault is at 100% of the line 54. Figure 3.12 shows the effective positive sequence impedance response calculated by the distance protection relay protecting Line 5-4 defined in equation (3.2). Figure 3.13 shows the logic outputs for fault dectector, distance elements and Out of Step Blocking (68B) element for this event.

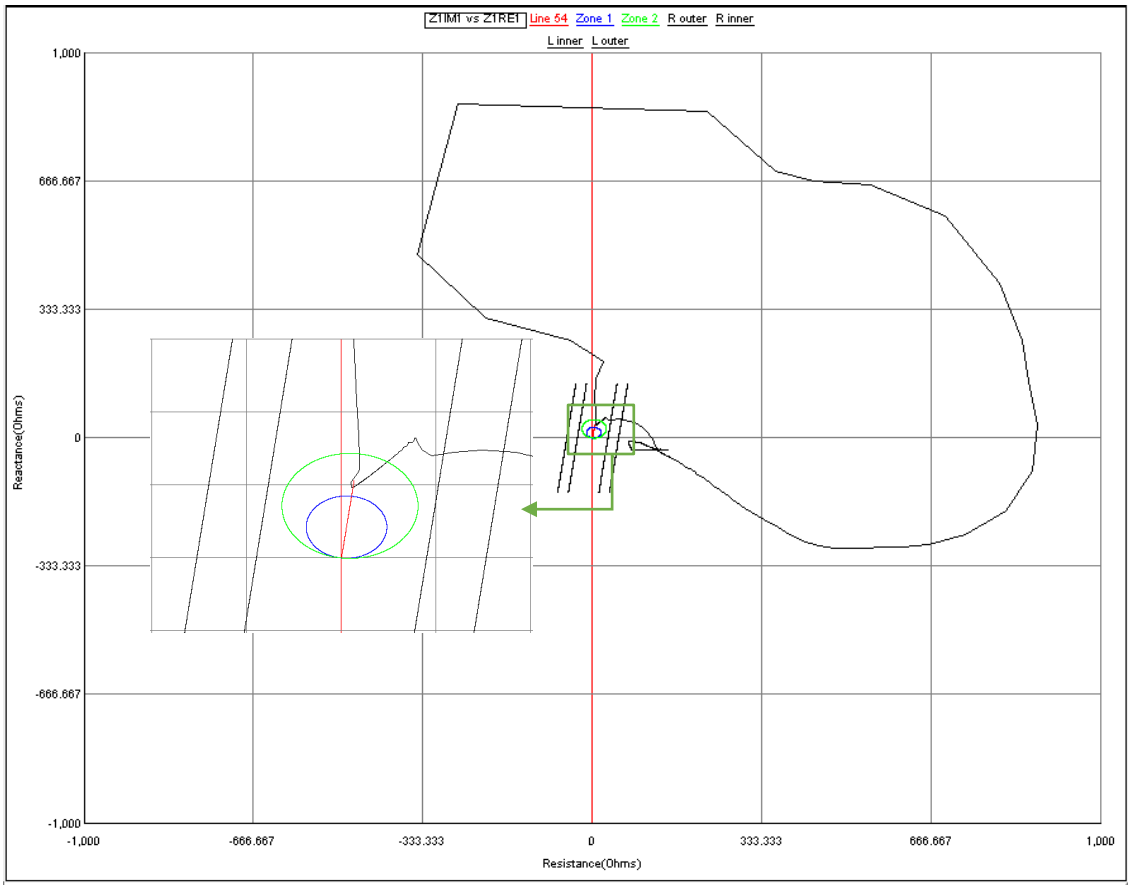

Figure 3.12: Positive Sequence Impedance (Z_1) Plane Plot - Case A

It is to be noted that only Zone 2 picks up for this fault because the impedance enters into Zone 2 operating characteristics of the distance relay before the timer for PSB expires. Therefore, the PSB classifies this event as fault and doesn't issue a PSB signal.

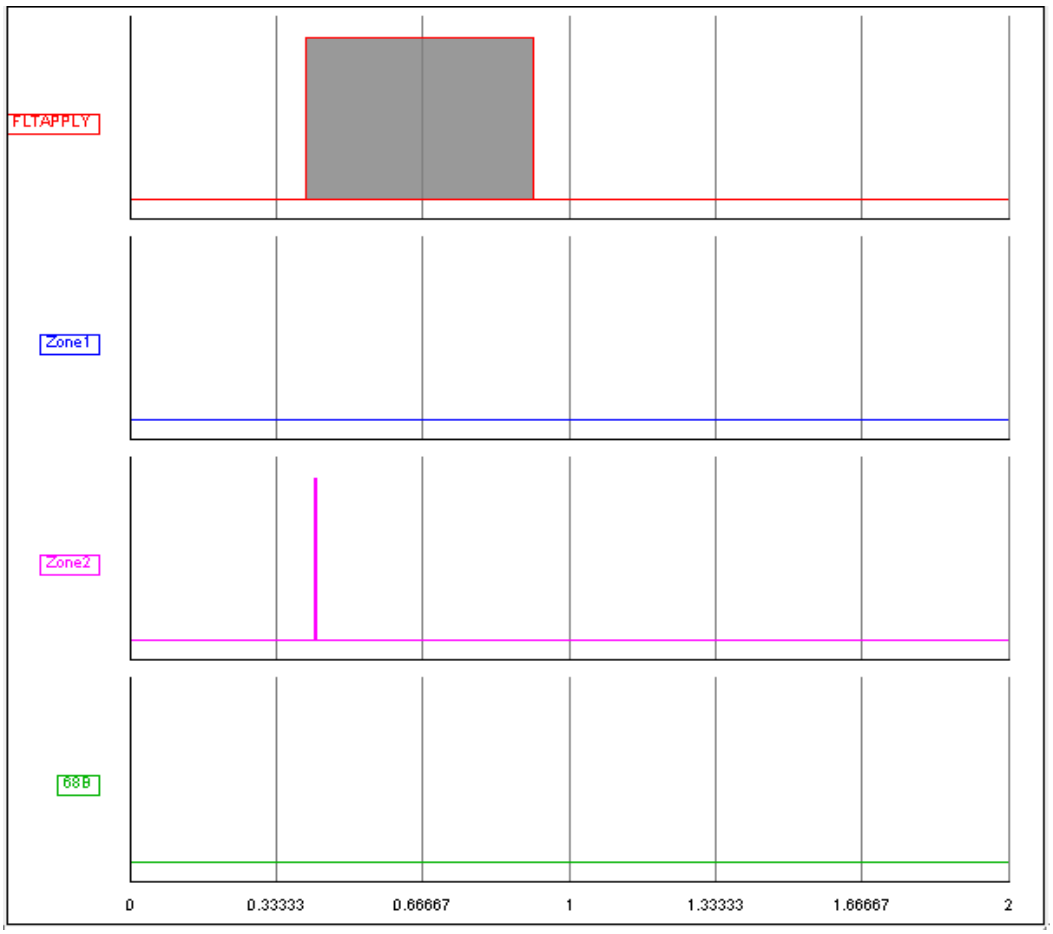

Figure 3.13: Logic Outputs for Fault detector, Distance Elements and Out of Step Blocking Element- Case A.

3.13.2 Case B: Three-Phase Fault at Bus 5

For a three-phase fault at Bus 5, the fault is initiated at the relay location on Line5-4. The impedance trajectory crosses the right side blinders and enters the distance element operating characteristics. The fault is at the relay location and the voltage seen by the voltage transformer is zero. As a result, the impedance seen by the relay during the fault duration is zero. The measured impedance crossed the concentric characteristics of Zone 1 and Zone 2 before the timer expires. The PSB classifies this event as a fault and does not issue a power swing blocking

signal. Figure 3.14 shows the impedance trajectory for this event and Figure 3.15 shows that the Zone 1 and Zone 2 fault elements correctly picked up for a fault at Bus 5.

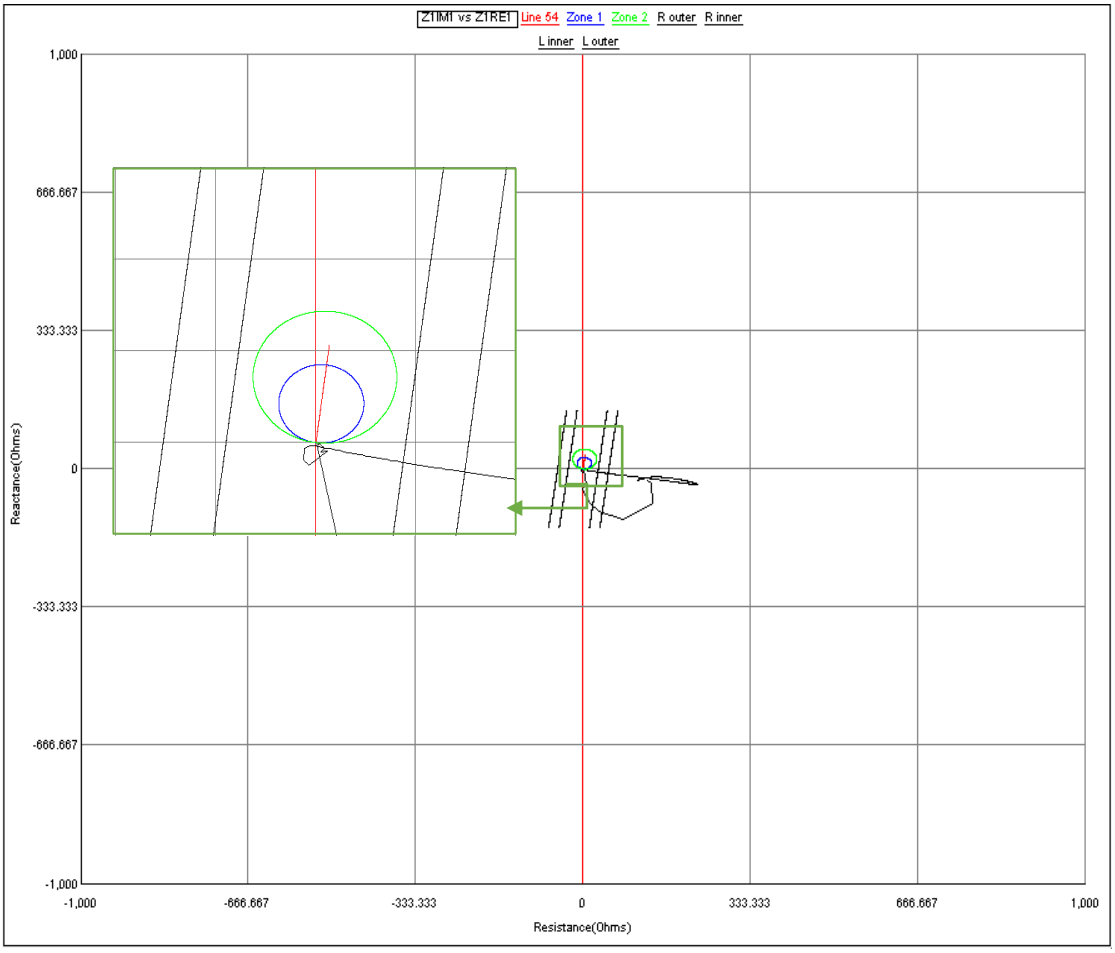

Figure 3.14: Positive Sequence Impedance (Z_1) Plane Plot- Case B

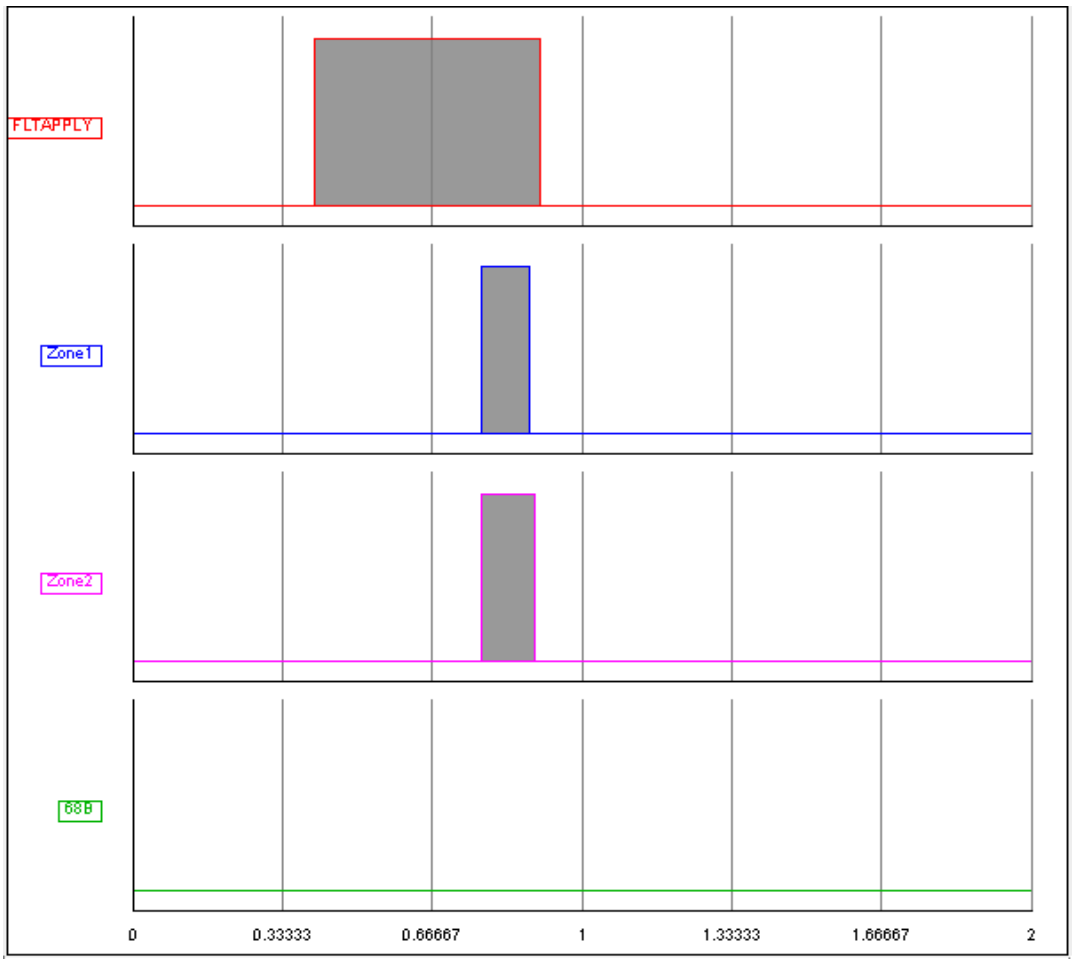

Figure 3.15: Logic Outputs for Fault Detector, Distance Elements and Out of Step blocking Element - Case B

3.13.3 Case C: Unbalanced Double-Line-to-Ground (BCG) Fault at Bus 3 (Fault Resistance= 0)

A BCG fault with fault duration equal to 0.5 s is induced at the Bus 3 in the 12-bus system shown in Figure 3.2. The distance element detects the event as a power swing and issues a PSB signal to block the operation of Zone 1 and Zone 2 of the distance elements. Figure 3.16 shows the effective impedance seen by the relay based on the voltages and currents shown in Figure 3.17. Note that the effective impedance initially crosses outer blinder and then moves back out,

and subsequently crosses both during the power swing after the fault is cleared. But the effective impedance does not enter Zone 2 for the relay.

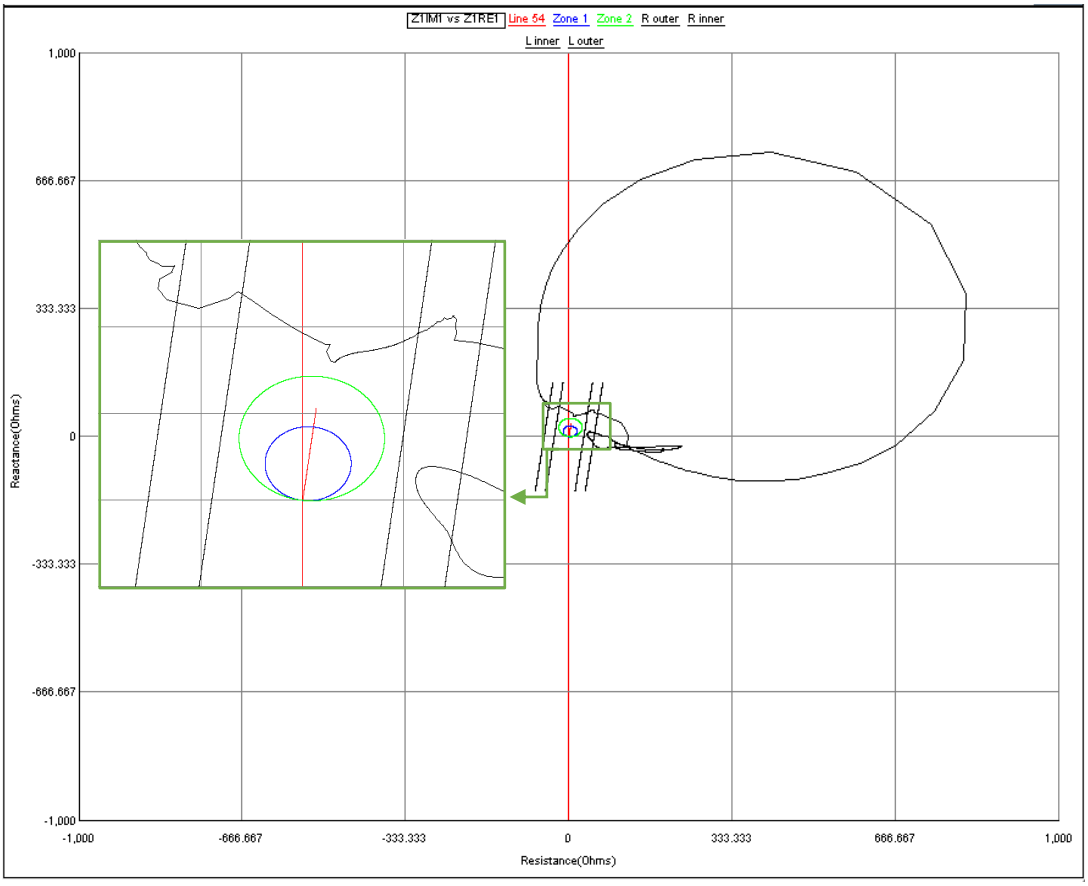

Figure 3.16: Positive Sequence Impedance (Z_1) Plane plot - Case C

Figure 3.18 illustrates the logic outputs for fault detector, distance elements and out of step blocking element for the unbalanced fault at Bus 3. During this event, there is a change in voltage and current values in B and C phases and A phase values remain unaltered during the fault and Figure 3.17 shows the voltage and current waveforms for the BCG fault at Bus 3 and the subsequent power swing that occurs after the fault is cleared. Note the low frequency envelopes around the 60 Hz voltages and currents during the power swing.

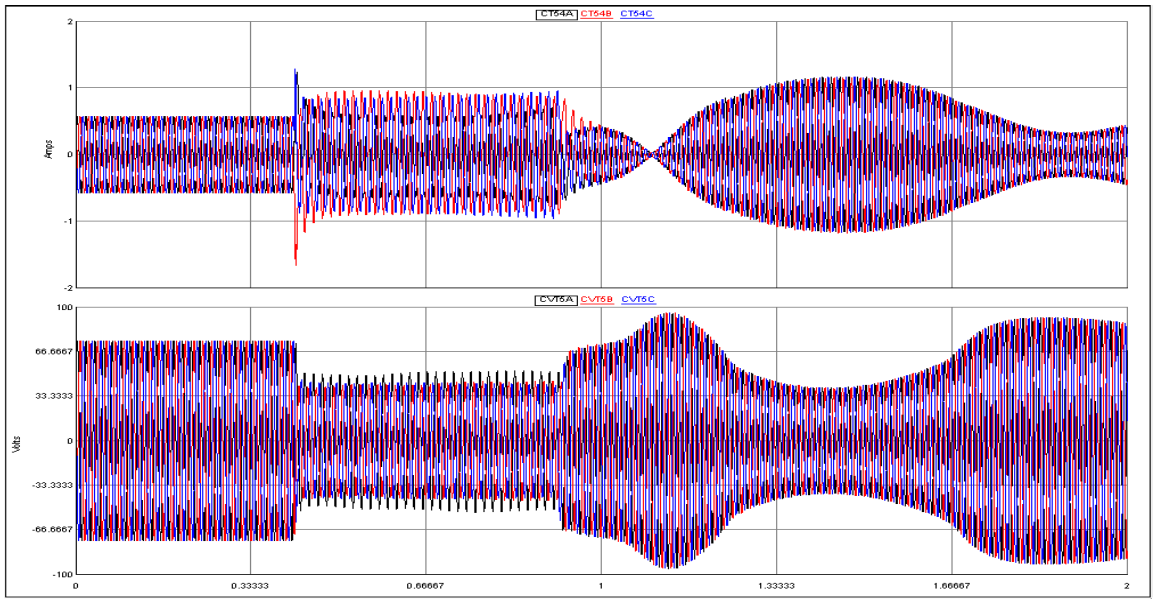

Figure 3.17: Current and Voltage Waveforms - Case C

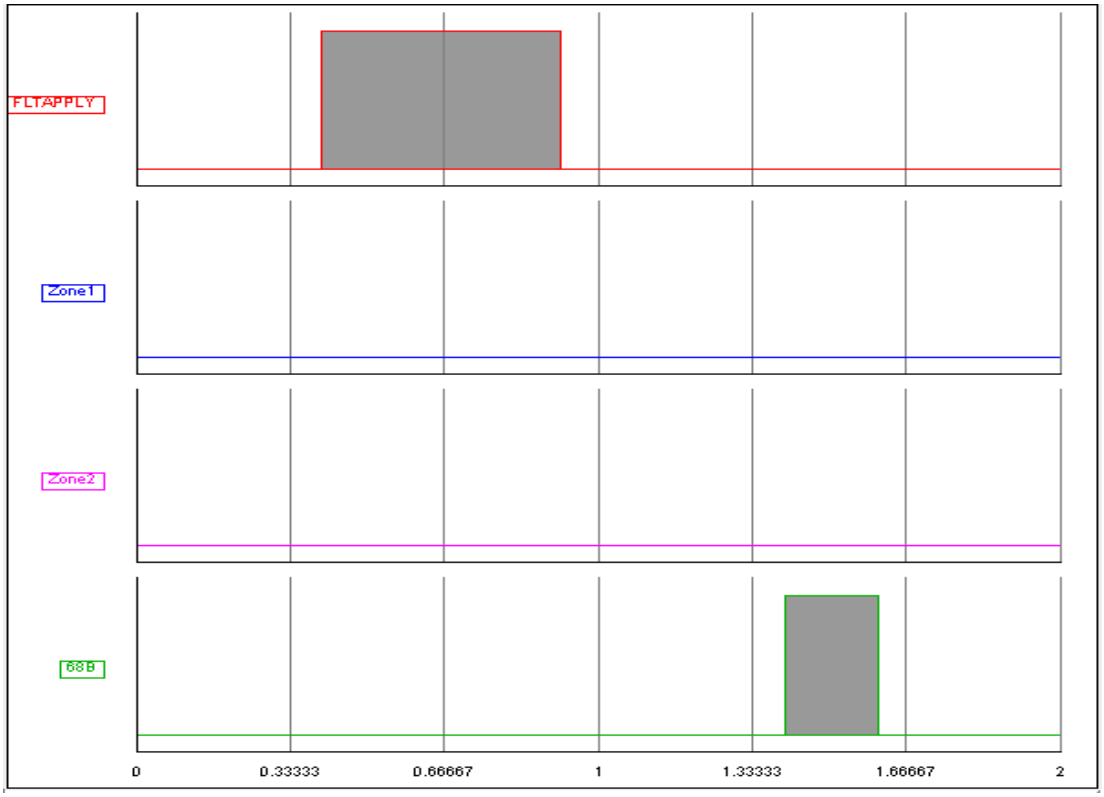

Figure 3.18: Logic Outputs for Fault Detector, Distance Elements and Out of Step Blocking Element - Case C

3.14. Summary

The complete test system with distance protection elements is implemented in RSCAD and discussed in this chapter. For the faults simulated at different buses, distance and power swing blocking functions operate correctly. The distance elements operate operate based on the fault location and their corresponding protection zone. The 68B function is shown to operate for stable power swings. This function blocks tripping be the relay.

The next chapter will look at the limitations of the conventional power swing protection schemes for systems with high penetration of renewable wind generation.

Chapter 4: Type 4 Wind Farm System Design

4.1 Introduction

Wind farms typically have a variable number of wind turbines. In the early 90's, many of the wind farms had wind turbine generators (WTG) of Type 1 (Type 1 WTG) which operate at constant speed. This type was coupled to the power system through a simple squirrel cage induction machine. This type of WTG requires reactive power, which was provided by compensating capacitor banks installed at the generator terminals. As wind hits the turbine blades, wind energy is transferred to the turbine for conversion to electricity. The rotor is coupled to the turbine via a gear box to step up its speed of rotation. Since there are no controllers, wind turbulence causes massive torque swings which reduced the life of the Type 1WTG. Type 2 WTG was developed subsequently to improve the operation. Its design employs the wound rotor induction machine with rotor winding coupled to a resistor bank. This design helps in achieving a better response for wind turbulence by allowing the generator speed to vary during the turbulence which reduced torque swings [9]. It still required a capacitor bank for local reactive power support.

Type 3 WTG's are the most commonly used design for present-day land-based installations. This type utilizes a doubly fed induction generator. Type 3 uses a wound rotor machine, which is similar to Type 2, except that the rotor is connected to a power converter that is coupled to the power grid through a second converter on the other side of a dc link. With the addition of the rotor side converter, reactive power output of the WTG can be controlled, and variable speed operation over a wider range of wind speeds is allowed. During faults in the power grid, the stator current of wound rotor machine increases resulting in high current transients in the rotor.

These current transients can cause heating of the power converter circuits. Therefore, older Type 3 WTGs have a crowbar circuit provided for the protection of the power converter to short-out the rotor and effectively changing the system to a Type 2 WTG when the currents exceed its rating. The crowbar protection impacts the currents that WTG can provide during short circuit conditions of Type 3 WTG.

Type 4 WTG's have a full rated power converter to interconnect the generator and the power system. The rotating machine is decoupled from the power system through a dc link. The design commonly uses either a permanent magnet synchronous machine or squirrel cage induction machine. The largest advantage of Type 4 compared to Type 3 WTG's is that variable speed operation without the need for a gear box, removing the most common point of failure of WTG. The main disadvantage is the higher cost of the power converter, as it is required to be fully rated. The short circuit characteristics depend on the control used in the power electronic interface. Typically, the maximum short circuit current must be limited to the 110-120% of the current rating of the converter to prevent the damage of the power electronic components [9]

This thesis builds on a previous work performed in modelling Type 4 WTG using PSCAD/EMTDC, which is described in [10]. Type 4 WTG design, controls are modelling in RSCAD and the impacts of the WTGs on power swing protection are studied on the IEEE 12-bus system. In the following sections, the design and the control operation of these machines and the implementation of the design in RSCAD are discussed.

4.2 Design Objective

The main objective of designing a Type 4 WTG system model is to simulate the response of the power electronic voltage source converter (VSC) to system faults when the synchronous

generator at Bus 11 is replaced with wind farm with a large number of Type 4 WTGs. This project will use a single equivalent WTG to represent the wind farm. The impact of the integrated Type 4 WTG system on the distance element response is studied for faults and power swings. A comparison between the response of distance element to faults between cases with high WTG penetration and conventional synchronous generator is presented.

4.3 System Description

The test system that is used for modeling Type 4 WTG is shown in Figure 4.1. The grid side converter for the WTG is connected to the 12-bus power system shown in Figure 3.2. The coupling transformer is used to integrate the generation into the AC system and is represented by its leakage reactance. The generator and generator side Voltage Source Converter (VSC) for the Type 4 WTG is not modeled in detail for this study. Instead, wind power that is being generated is injected to dc bus as a controlled DC voltage source. Reference [10] discusses the design of Type 4 WTG developed in PSCAD/EMTDC and is used as a basis for model development to study the behavior of Type 4 WTG in RSCAD. A power system can have many wind turbines, but for this study, a single turbine with a rating equivalent to that of the synchronous generator connected to Bus 3. The details of the system design are given in the following sections.

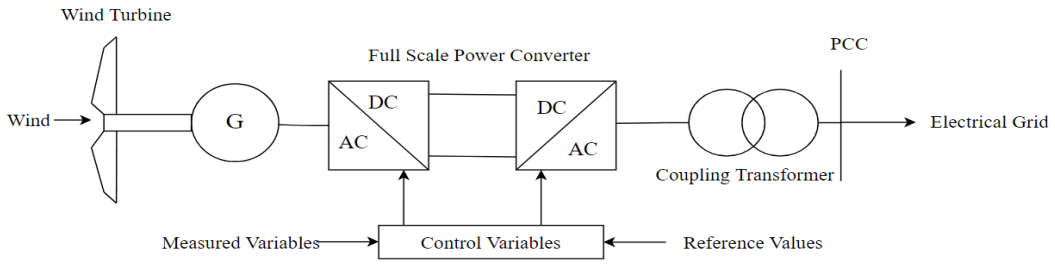

Figure 4.1: Configuration of Type 4 Wind Turbine System

4.4 Structure of the Grid Side Converter

The advantages of the power electronic-based Voltage Source Converters are the controls used to maximize the active output power while also having the option to manage the reactive power exchange with the grid for voltage regulation on the AC grid. The grid side converter used is a three-phase, two-level voltage source converter shown in Figure 4.2. R and L in the Figure 4.2 are the resistance and inductance between the power converter output terminals and power grid. The switches are numbered S1-S6, in their switching sequence order during one cycle in 6-step operation.

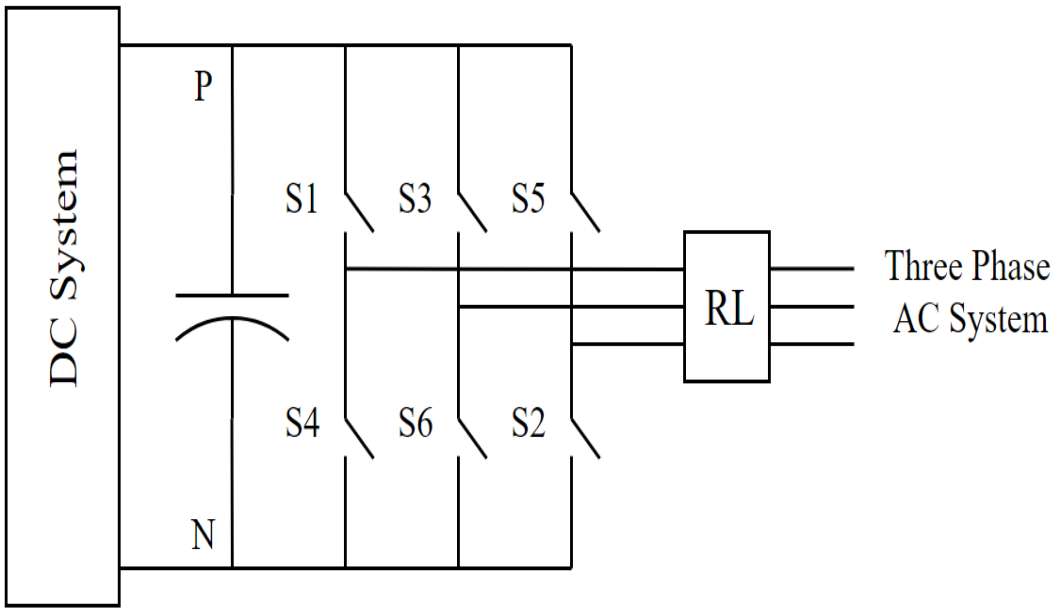

Figure 4.2: Schematic Diagram of a Three-Phase, Two Level VSC

The converter operates based on the alternate switching of the power electronic devices, which are controlled to supply the three-phase voltage synchronized to the grid frequency. The control scheme used is Pulse Width Modulation (PWM) technique, as explained in the next section [11]. The switching model represents the steady-state and dynamic behavior of the converter

along with an approximation of the high frequency behavior due to the switching. The accuracy can be increased if more elaborate model is used for the power circuit components, for example more accurate switch models, which would also require a time-step in the tens of nanoseconds. Using a switching function for the transistors, the instantaneous values of current and voltage variable can be determined by the switching model. These variables include high frequency components due to switching process and as well has slow transients.

The modulating signal which is the primary control variable of the converter, impacting the currents and voltages, controls fundamental frequency response of the converter. For the purpose of conducting a dynamic analysis and designing controls, the knowledge of the high-frequency details of the current and voltage variables is not needed. Furthermore, we are interested in the dynamics of the low frequency values rather than the instantaneous values of currents and voltages. Therefore, an average model is developed from reference [10] and is used to describe the converter dynamics as a function of the modulating function. Use of this model allows simulating the system with a standard 50 microsecond time step in the RTDS.

4.5 Pulse Width Modulation Technique

The principle of the pulse width modulation (PWM) technique is the control of the gating pulses for the power electronic devices of the converter to track the essential magnitude and angle at the fundamental frequency. The detailed explanation of this technique is presented in [11] and is shown using a simple schematic diagram given in Figure 4.3. The sinusoidal waveform shown in the Figure 4.3 is the modulating signal and the triangular waveform is referred to as

carrier signal which is normalized to -1 to +1. The triangular wave frequency is generally much higher than the modulating signal.

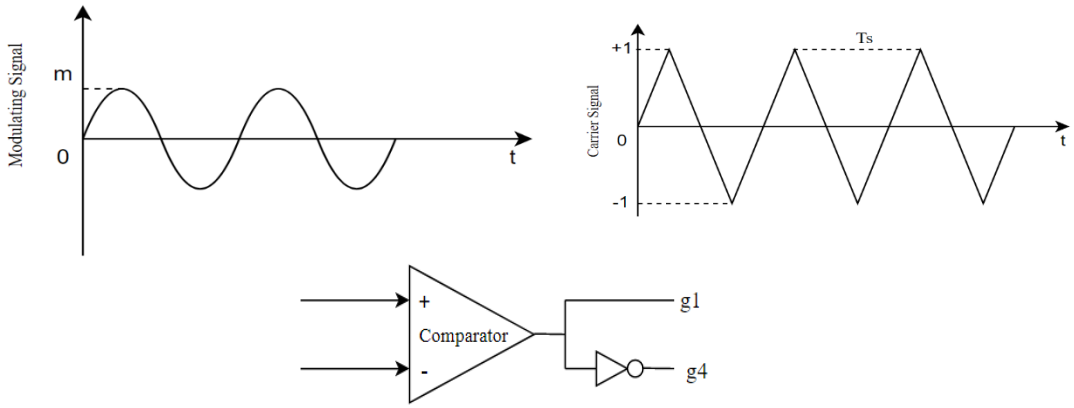

Figure 4.3: Schematic Diagram Showing Pulse Generation by Pulse Width Modulation Technique [11]

The intersections of the carrier and the modulating signals determine the switching instants of the power electronic devices. This is can be described by considering one leg of VSC with switching devices S1 and S4, if the magnitude of the modulating signal is higher than the carrier signal; a gate pulse g1 is issued to turn-on the switch S1 and a gate pulse g4 to turn off switch S4 which is illustrated in Figure 4.4. Based on the switches that are ON at a given instant, the ac side of the VSC terminal voltage is either $\frac{V_{DC}}{2}$ or $-\frac{V_{DC}}{2}$. The PWM controls are designed in such a way that the output voltages in the system are plotted they have a fundamental frequency of 60 Hz.

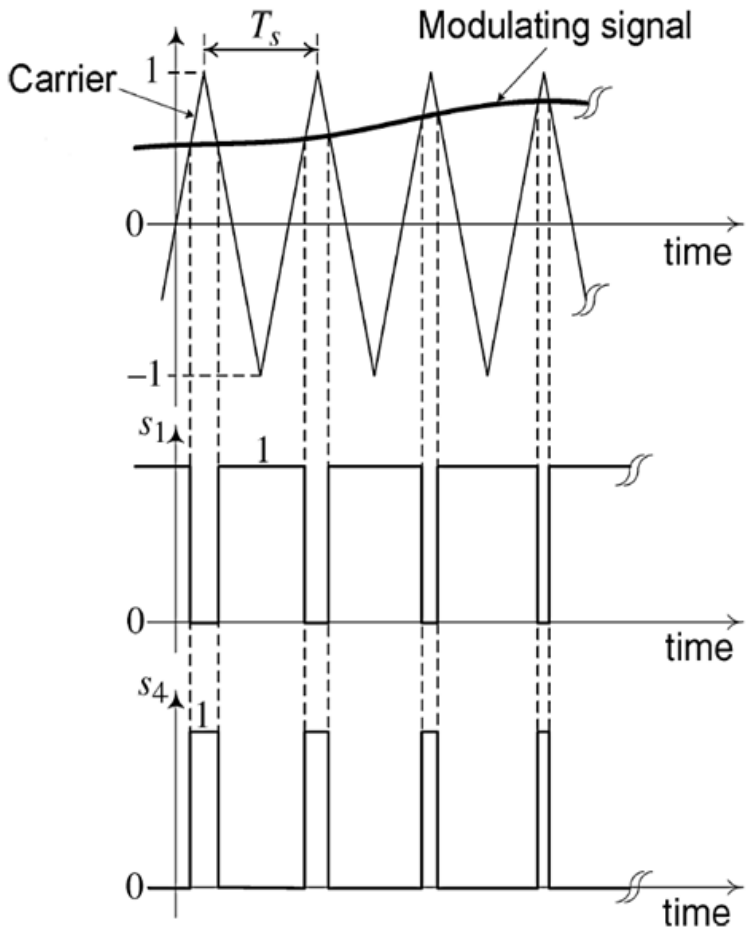

Figure 4.4: PWM Based Switching of S1 and S4 [11]

The equations representing the switching functions for S1 and S4 are given below

$$s_1(t) = d(t) \tag{4.1}$$

$$s_4(t) = 1 - d(t) \tag{4.2}$$

Where, *d(t)* is the duty ratio or the fraction of T_s when S1 is ON.

It is to be noted that from Reference [11], the two switches must be ON at the same time to prevent a short-circuit of the DC bus capacitor. The condition could be mathematically summarized by the following equations;

$$s_1(t) + s_4(t) = 1 \tag{4.3}$$

$$V_t\,(t) = \left[\frac{V_{DC}}{2} * s_1(t)\right] - \left[\frac{V_{DC}}{2} * s_4(t)\right] = \frac{V_{DC}}{2}\left[s_1(t) - s_4(t)\right] \tag{4.4}$$

$$i_p(t) = i * \ s_1(t) \tag{4.5}$$

$$i_n(t) = i * \ s_4(t) \tag{4.6}$$

Where i_p and i_n are the current flowing in S1 and S4, respectively.

4.6 Park's Transformation for Inverter Controls

It is common to perform closed-loop regulation of the ac current outputs from the converter. However, the three-phase instantaneous quantities are time-varying at the power system frequency, which results in a complex regulator design. The Park's transformation to the synchronous reference frame is often used to simplify the calculation for the controls of three-phase converter circuits. This transformation converts the three-phase AC results into two-axis reference frame rotating quantities at system frequency, which are at zero frequency in steady-state. The two axes are labelled as the direct axis (D), quadrature axis (Q). There is also a common mode term (0) which is a zero-sequence term.

The DQ0 transformation is explained in the following discussion. Consider a set of balanced three-phase sinusoidal functions as follows

$$f_a(t) = \bar{f}\,cos(\omega t) \tag{4.7}$$

$$f_b(t) = \bar{f}\,cos\left(\omega t - \frac{2\pi}{3}\right) \tag{4.8}$$

$$f_c(t) = \bar{f}\,cos\left(\omega t + \frac{2\pi}{3}\right) \tag{4.9}$$

Where, $\bar{f}$ is the peak amplitude of the phasor, ω is the frequency of the phasor in rad/sec.

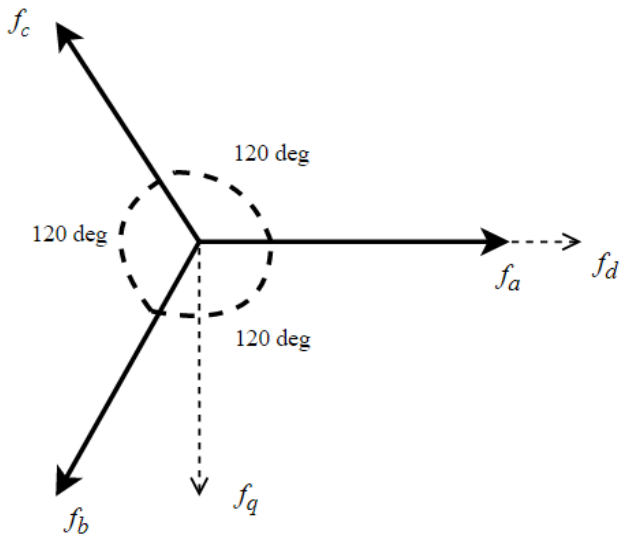

Figure 4.5: Phasor Representation of a Set Balanced Three-Phase Quantities

These quantities are reassigned into a set of two orthogonal vectors f_d and f_q which are shown in Figure 4.5 and calculated using equation (4.10)

$$\begin{bmatrix} f_d \\ f_q \end{bmatrix} = \frac{2}{3}\begin{bmatrix} cos\theta & \cos\left(\theta-\frac{2\pi}{3}\right) & \cos\left(\theta+\frac{2\pi}{3}\right) \\ sin\theta & \sin\left(\theta-\frac{2\pi}{3}\right) & \sin\left(\theta+\frac{2\pi}{3}\right) \end{bmatrix}\begin{bmatrix} f_a \\ f_b \\ f_c \end{bmatrix} \tag{4.10}$$

Where, θ is the transformation angle, which can be or a function of time.

The value θ is the reference angle for the transformation, which can be a constant for a stationary reference frame or ωt for a rotating reference frame. In this research, θ is rotating based on the power system frequency. A Phased Locked Loop (PLL) is used to tracks the system frequency from the voltages measured at PCC. The converter controls are designed to trace this reference frequency, such that f_d and f_q are DC quantities in steady state. This transformation synchronizes the converter quantities to a rotating reference frame. Using equation (4.10), and

an accurate measurement of the angle θ, synchronization can be controlled such that f_d is made to trace the peak magnitude of the reference quantity and f_q quantity can be made close to zero.

In this work, V_a, the phase A voltage at the point of common coupling (PCC) shown in Figure 4.1is the reference quantity. The peak amplitude of V_a is $V_{sd,}$ and the synchronization is controlled in such a way that V_{sq} at the converter terminal is regulated to zero when synchronized. This simplifies the control design for the VSC and allows the decoupling between the real and reactive power for both converters. DQ0 transformation for the voltage and currents implemented in RSCAD with built-in model blocks for DQ transformation are presented in Figure 4.6 and 4.7

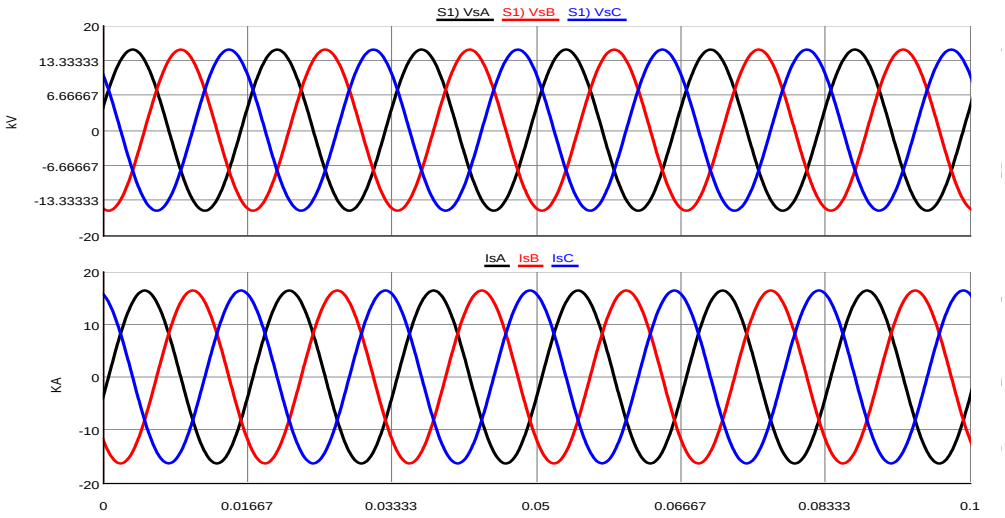

Figure 4.6: Voltage and Current Waveforms at Point of Common Coupling

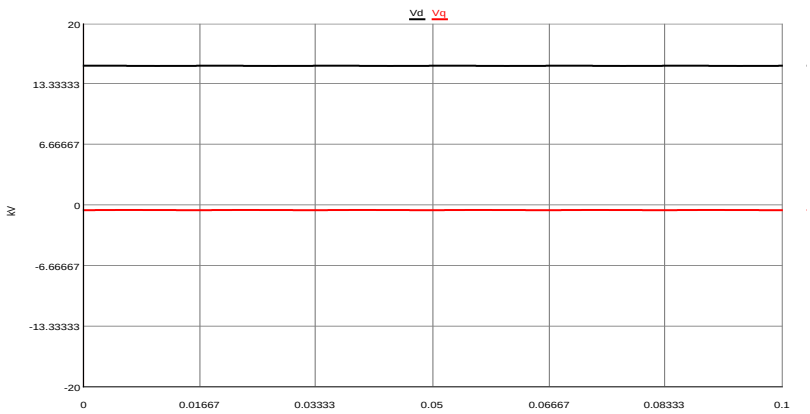

Figure 4.7: DQ Frame Quantities of Converter Terminal Coltages

4.7 Average Non-Switching VSC Model

Figure 4.8 gives a schematic diagram of a non-switching model of the VSC system. Reference [11] presents the method of deriving the non-switching average model to perform studies related to the low frequency dynamics and control of the converter. From Figure 4.8, the ac current on one phase between the converter terminal and the ac side connected to the Bus 3 is given by the equation

$$L\frac{d}{dt}i(t) + Ri(t) = V_t(t) - V_s \tag{4.11}$$

Where, L is the equivalent inductance of the system between VSC terminal and PCC

R is the equivalent resistance between the VSC terminal and the PCC

V_s is the AC voltage at PCC

V_t is the AC side terminal voltage of the VSC which is a periodic function with time period T_s

According to [11], if the switching frequency ω_s is larger than R/L, the periodic component of the input has a negligible contribution to the entire output and hence, it can be assumed that $i(t) = \bar{\imath}(t)$. The voltage at the converter terminals is the function of the modulating function for that phase and it is half of the DC Voltage [11].

$$\bar{V}_t = \frac{V_{DC}}{2}(2\,d(t) - 1) \tag{4.12}$$

$$\bar{\imath}_p = i * d(t) \tag{4.13}$$

$$\bar{\imath}_n = i * (1 - d(t)) \tag{4.14}$$

Using the PWM technique, $m(t) = 2\,d(t) - 1$ gives the relationship between the modulating function and the duty ratio. The value of *d* varies from 0 to 1 as *m* changes from -1 to +1.

Replacing $d(t)$ in the equations (4.12) to (4.14) with $d(t) = \frac{1}{2}[m(t) + 1]$ results in the following equations

$$\bar{V}_t = m(t) * \frac{V_{DC}}{2} \tag{4.15}$$

$$\bar{\imath}_p = \frac{(1+m(t))}{2} * i \tag{4.16}$$

$$\bar{\imath}_n = \frac{(1-m(t))}{2} * i \tag{4.17}$$

The average power per phase at the DC bus and the AC side of the converter terminal derived using equations (4.15) to (4.17) are given as:

$$\bar{P}_{DC} = \frac{V_{DC}}{2} * \left(\bar{\imath}_p + \bar{\imath}_n\right) = m(t) * \frac{V_{DC}}{2} * i \tag{4.18}$$

$$\bar{P}_t = \bar{V}_t * i = m(t) * \frac{V_{DC}}{2} * i \tag{4.19}$$

The AC side power at the Point of Common Coupling at Bus 11 is given as

$$P_s(\mathrm{t}) = V_{s^*} i \tag{4.20}$$

The average circuit equivalent model of the ideal three phase two-level VSC derived from equations (4.15) to (4.20) is shown in Figure 4.8.

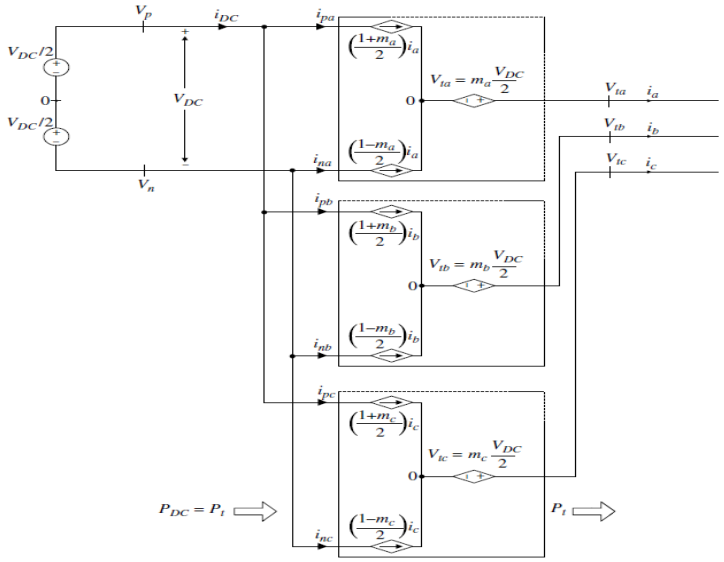

Figure 4.8: Averaged Equivalent Circuit Model of an Ideal Two-Level VSC [11]

The average circuit model of the VSC converter modeled in RSCAD is shown in Figure 4.9

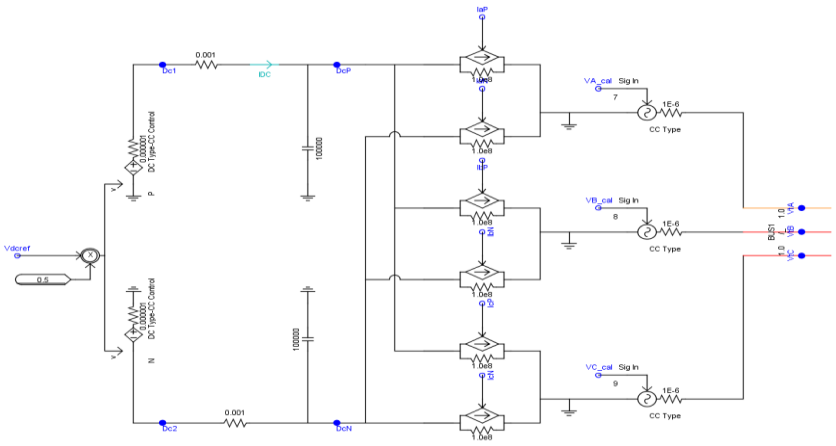

Figure 4.9: Averaged Equivalent Circuit of Grid Side VSC Modeled in RSCAD

4.8 Voltage Droop Controller

The controls of the Type 4 WTG regulate the turbine power close to get the maximum power for the wind speed. Since the thesis is modeling only the grid side converter, constant power in injected to the DC link representing the output from the machine side converter. In order to transfer maximum power to the ac system, the grid side converter regulates the dc-link capacitor voltage to a set reference value. A voltage droop control is added for controlling the voltage and it is given in equations (4.20) with the dc voltage reference defined in (4.21)

$$Droop = \frac{P_{const} - P_{DC}}{P_{const}} \tag{4.20}$$

$$V_{DCref} = V_{DCconst} + Droop \tag{4.21}$$

Where, P_{const} is the desired power from the WTG maximum power point tracking,

P_{DC} is the average power at the DC bus terminals,

$V_{DCconst}$ is the desired constant DC voltage,

V_{DCref} is the reference voltage.

The voltage droop controller model as implemented in RSCAD is shown in Figure 4.10

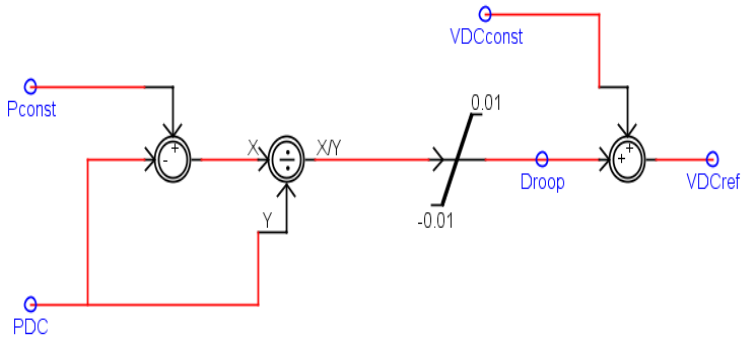

Figure 4.10: Voltage Droop Controller Model Implemented in RSCAD

4.9 Outer DC Voltage Control

One important control objective is to regulate the dc bus voltage V_{DC}. The outer controller is referred to as the dc bus voltage compensator in reference [11]. In this thesis, the generator mechanics of the wind turbine and the generator side converter are not modeled, as the scope is to study the behavior of the distance element relay under the faulted conditions in the 12-bus System. The grid side of the WTG uses a current controller where real/reactive power output of the VSC is controlled by setting current reference values for the current regulator. The generator side VSC is represented by a constant dc source at the dc link capacitors. This assumption is acceptable if the system operates in steady state. During fault conditions, power imbalances occur in the system leading to the large variations of the dc bus voltage and entire WTG which are either regulated using the generator side VSC controls or a resistive chopper circuit [11]. Neither are represented in this thesis. Therefore, for fault study analysis, the generator side of WTG is represented by the controlled DC voltage source.

Figure 4.11 illustrates the controlled dc voltage port implemented in RSCAD. To regulate the dc bus voltage, a feedback mechanism is used where V_{DC} across the capacitors is compared with the reference voltage command and a PI controller adjusts P_{ref} accordingly, such that the net power exchanged with the dc-link capacitor is kept zero. The error signal is sent through a PI controller and the output signal P_{ref} is maintained within the setpoint value.

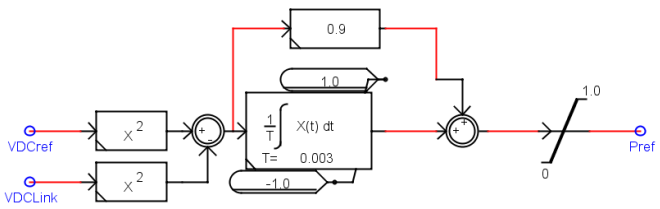

Figure 4.11: DC Bus Voltage Controller Modeled in RSCAD

4.9.1 Current Reference Generator

The role of the inner control loop is to produce modulating signals m_a , m_b and m_c for the PWM generator. The current regulator is implemented in the synchronous DQ reference frame. The outputs of the outer control loop I_{dref} and I_{qref} derived from P_{ref} and Q_{ref} are used as the inputs and compared with the measured currents at the AC side terminals. The reference currents equations are generated based on the following equations. It is known that the complex power is the product of the voltage and the conjugate of the current and is given below

$$P + jQ = \frac{3}{2} * \vec{V} * \vec{I}^{*} \tag{4.22}$$

Applying parks transformation to the three-phase voltage and currents and substituting in the above equation we get

$$PT(t) = \frac{2}{3}\begin{pmatrix} \frac{1}{2} & \frac{1}{2} & \frac{1}{2} \\ \cos(\theta(t)) & \cos(\theta(t) - \frac{2\pi}{3}) & \cos(\theta(t) + \frac{2\pi}{3}) \\ -\sin(\theta(t)) & -\sin(\theta(t) - \frac{2\pi}{3}) & -\sin(\theta(t) + \frac{2\pi}{3}) \end{pmatrix} \tag{4.23}$$

$$V_{0DQ}(t) = PT(t)\begin{pmatrix} V_a(t) \\ V_b(t) \\ V_c(t) \end{pmatrix} \tag{4.24}$$

$$I_{0DQ}(t) = PT(t)\begin{pmatrix} I_a(t) \\ I_b(t) \\ I_c(t) \end{pmatrix} \tag{4.25}$$

Separating the real and reactive power in the equation after transformation is given in

$$P = \frac{3}{2} * \left(V_d I_d + V_q I_q\right) \tag{4.26}$$

$$Q = \frac{3}{2} * \left(V_q I_d - V_d I_q\right) \tag{4.27}$$

Defining the reference for V_d to align with the positive peak $V_a(t)$ at the point of interconnect is achieved by regulating V_q to zero. This result also simplifies (4.26) and (4.27).

Rearranging the above equations to obtain the I_{dref}, I_{qref} from P_{ref} , Q_{ref}

$$I_{dref} = \frac{2}{3}\left(\frac{P_{ref}}{V_d}\right) \tag{4.28}$$

$$I_{qref} = \frac{-2}{3}\left(\frac{Q_{ref}}{V_d}\right) \tag{4.29}$$

The implementation of the reference current generator in RSCAD is shown in Figure (4.12)

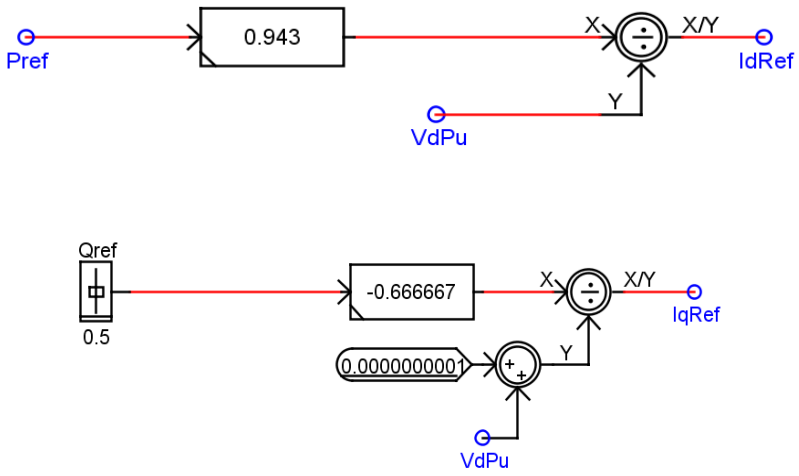

Figure 4.12: Reference Current Generator in RSCAD

The reactive power Q_{ref} is controlled independently [11]. In many applications Q_{ref} is zero as the owner of the wind farm is not compensated for supplying reactive power.

4.9.2 Inner Current Control Loop

The main objective of this current control loop is to provide fast control of the currents, including limiting converter currents during ac faults. As described above, in this work it is used regulate the real and reactive power that the grid side VSC of the WTG supplies to the ac

system. The study implements current mode control to regulate the real and reactive power, where the VSC output currents are regulated by controlling fundamental frequency components of the converter terminal side voltages. The phase angle and the amplitude of the currents relative to the voltage at the point of common coupling (PCC) regulate the real and reactive power injected at the PCC. The Kirchhoff's Voltage loop equation for the AC circuit is given by the following equation

$$V_s = -L\frac{d}{dt}i(t) - Ri(t) + V_t \tag{4.30}$$

For the inner control loop, the proportional-integral compensator is used, the integral term of the compensator ensures that the reference values are closely tracking to guarantee that the steady-state error is zero. The compensator processes the error signal and is maintained which in limits and delivered to the converter for generating Pulse Width Modulating signal. The control loop diagram implemented in RSCAD is given in Figure 4.13.

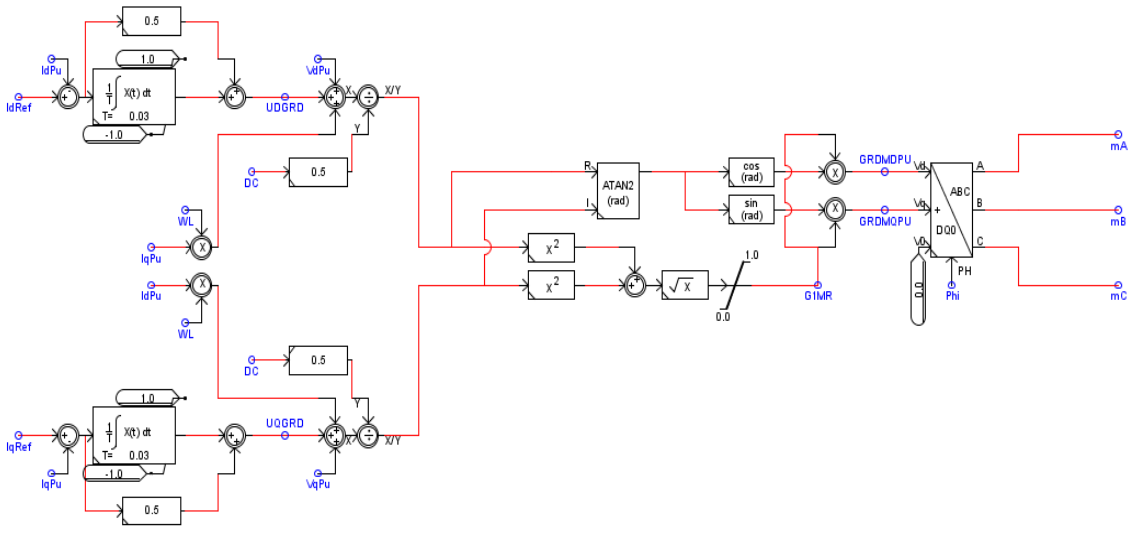

Figure 4.13: Inner Current Controller as Implemented in RSCAD

The voltages and currents at the point of interconnect in steady-state operation are given in Figure 4.14

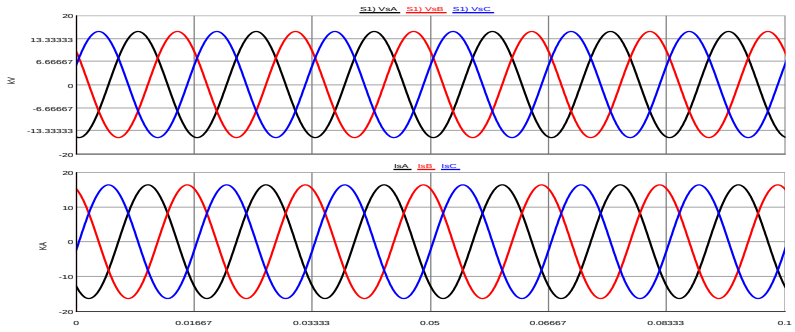

Figure 4.14: Steady-State Voltage and Current of Type 4 WTG at the Point of Interconnect

4.10 Comparison of the Performance of Large WTG Installation with Synchronous Machine

Before studying the effect of Type 4 WTGs on the system protection function, it is necessary to know the difference in operation in response to major disturbances compared to a system with only synchronous machines. Different types of faults are simulated in the 12-bus test system, and the voltage at the point on interconnect is plotted in each of the fault cases. The duration of the fault is 0.1 sec at each location. That means the fault is initiated and the circuit breaker clears the fault in 0.1 sec.

4.11 Fault Case: Three Phase Fault at Bus 7

The voltage and current waveforms of the at the point of interconnection of the wind generation system are shown in Figure 4.15. It can be clearly observed that the Type 4 WTG has an initial transient overcurrent following the inception of fault, and then transitioned to steady-state fault current. This scenario is different in the synchronous based generation which has three stages of response during the fault- sub-transient, transient and steady-state. Figure 4.16 shows the

voltage and current response for a fault at Bus 3 with a synchronous machine producing power instead of the aggregated equivalent Type 4 WTG.

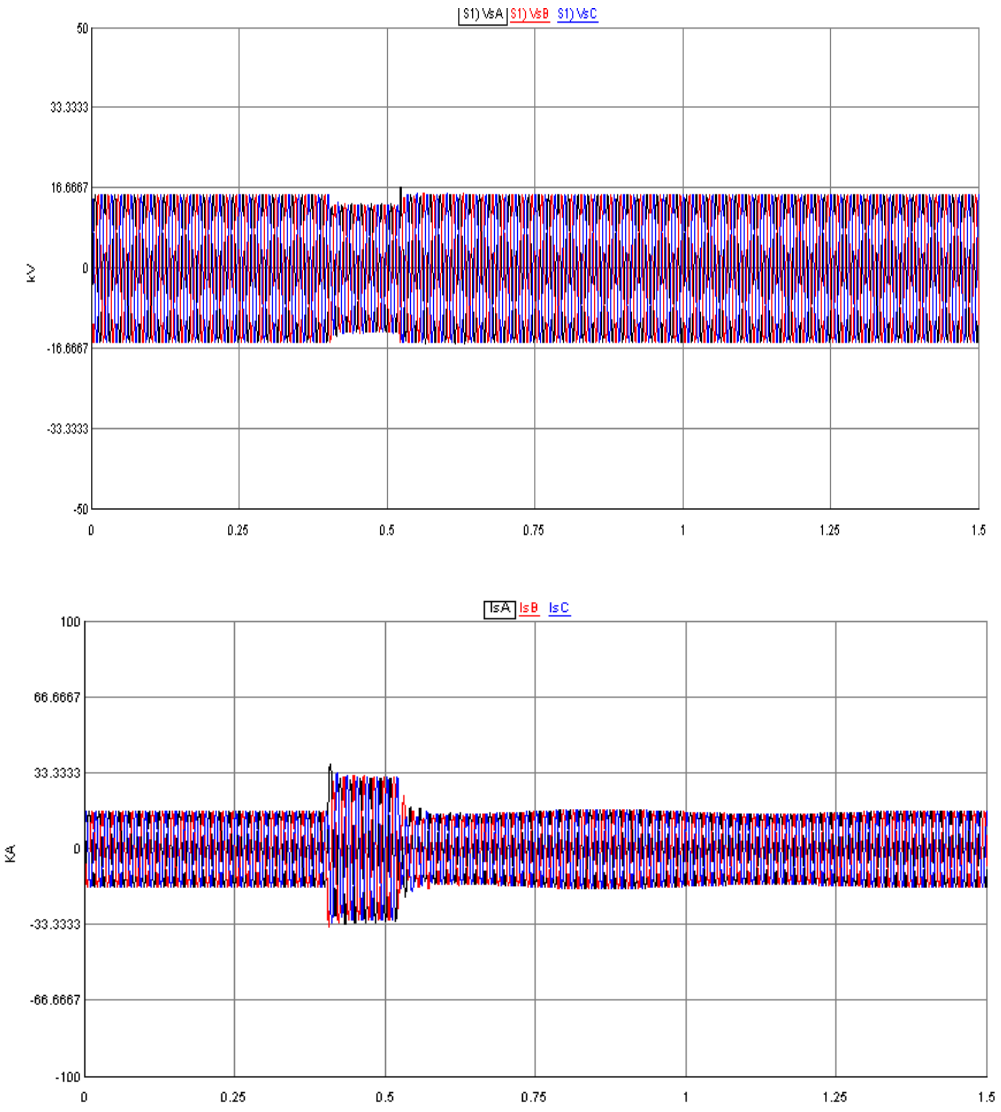

Figure 4.15: Voltage and Current Waveforms of Type 4 WTG Following the Inception of a Fault

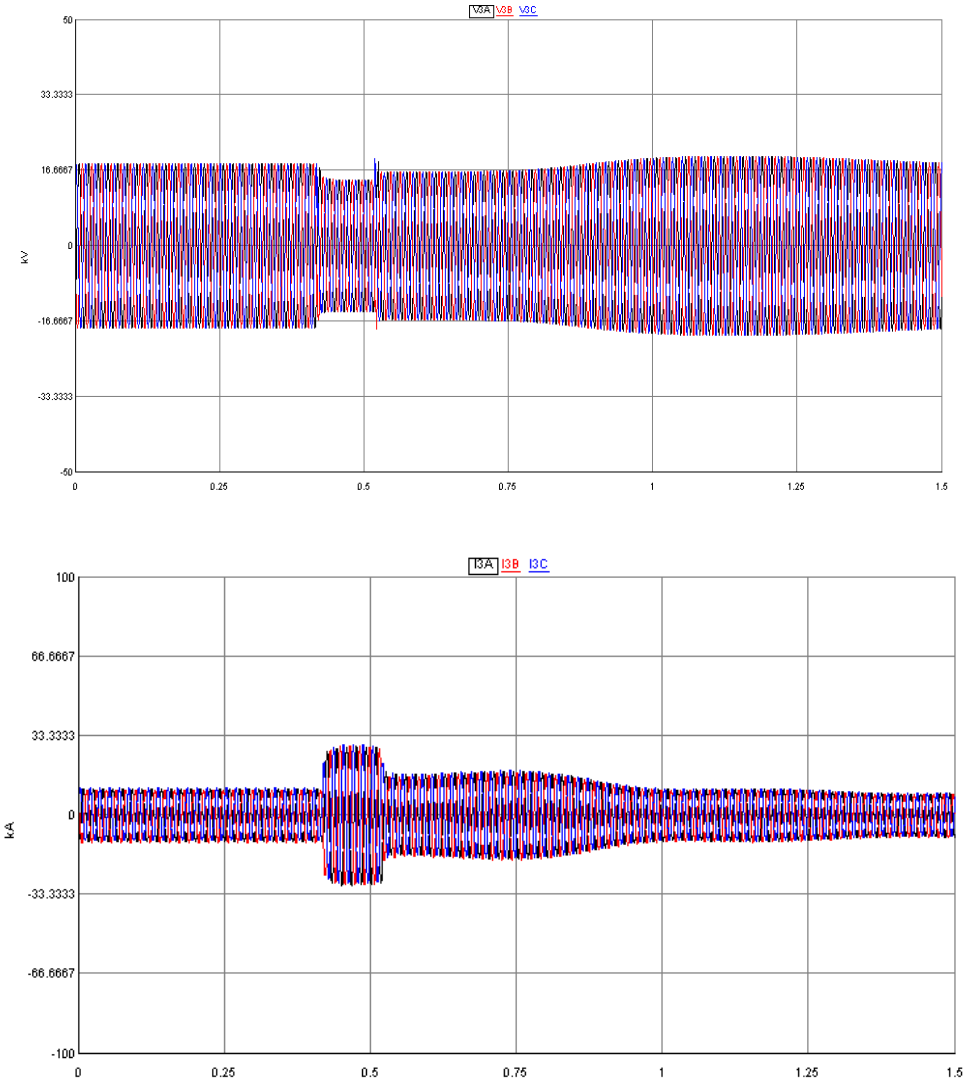

Figure 4.16: Voltage and Current Waveforms at Bus 3 with Synchronous Generator following the Inception of a Fault

The voltage and current waveforms from Figure 4.15 show the indirect impact of the WTG controller varying the voltage to limit the currents to 1.2pu when there is a fault in the system. The currents supplied by the WTG, which is represented by the controlled DC source is almost constant; there is only a small change in WTG currents in response to the fault. It is because the control is responding fast to bring the current within the limits.

4.11 Fault Response Simulation Cases with Wind Generation

The fault cases discussed in Chapter 3 are simulated again to analyze the response of the distance protection with wind generation systems replacing the large synchronous machine at Bus 3 with Type 4 WTG. In all the fault simulation cases, the fault resistance, R_f, is zero.

4.11.1 Case A: Three Phase Fault at Bus 4

A three phase to ground fault is applied on Bus 4 which falls in the Zone 2 element coverage. This event results in changes in voltages and currents. The impedance calculated by the distance

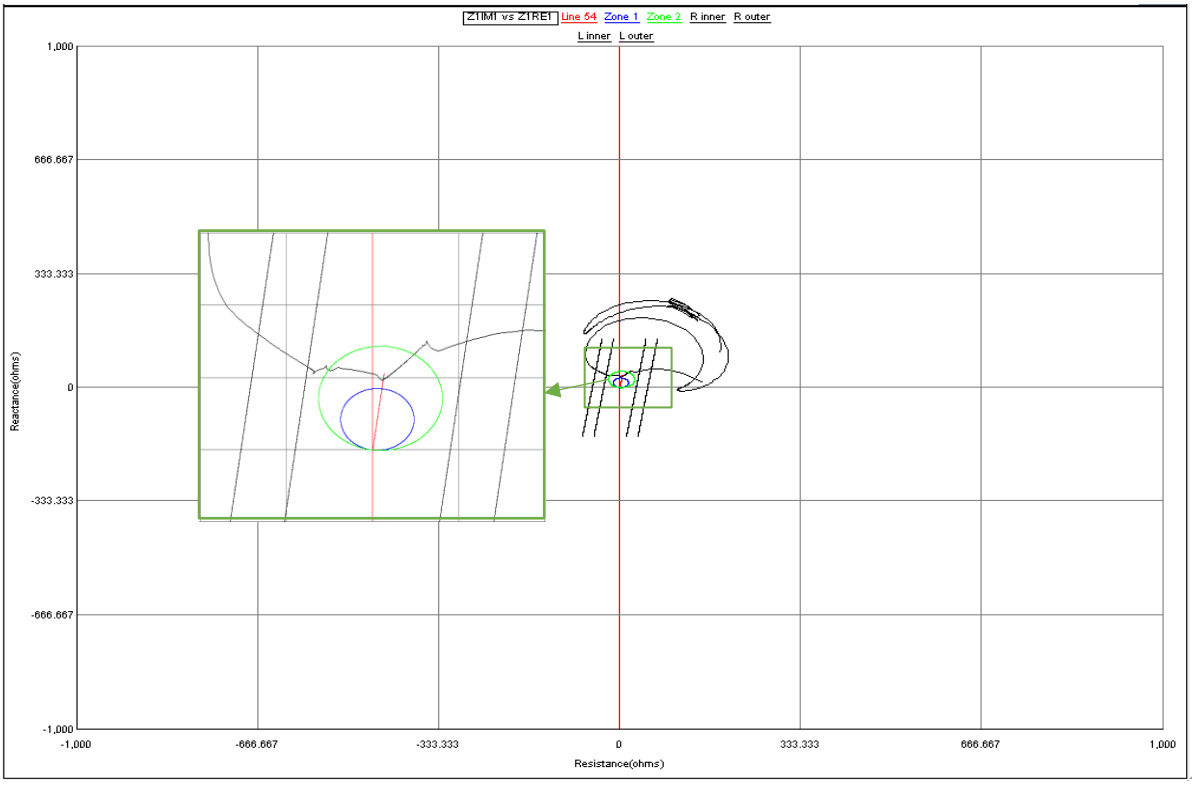

Figure 4.17: Positive Sequence Impedance (Z_1) Plane Plot - Case A

element enters the right hand blinders and enters zone 2 operating characteristics. As discussed earlier, the systems with large penetration of wind generation experience increased rates of change of the positive sequence impedances seen by the relay.

When this event is simulated under no wind conditions, the impedance trajectory entered the distance element zone 2 coverage and the zone 2 element picked up. But with wind generation, the impedance crosses the inner right side blinders and enters the inner left side blinders after the fault is initiated. This results in the Out of Step element mistakenly issuing an OST signal declaring an unstable swing. Although the positive sequence impedance enters the zone 2 operating characteristics, due to the faster rate of change of impedance the zone 2 element doesn't pick up. It is because, the timer set for detecting OST is greater than the time delay set for detecting faults in Zone 2.

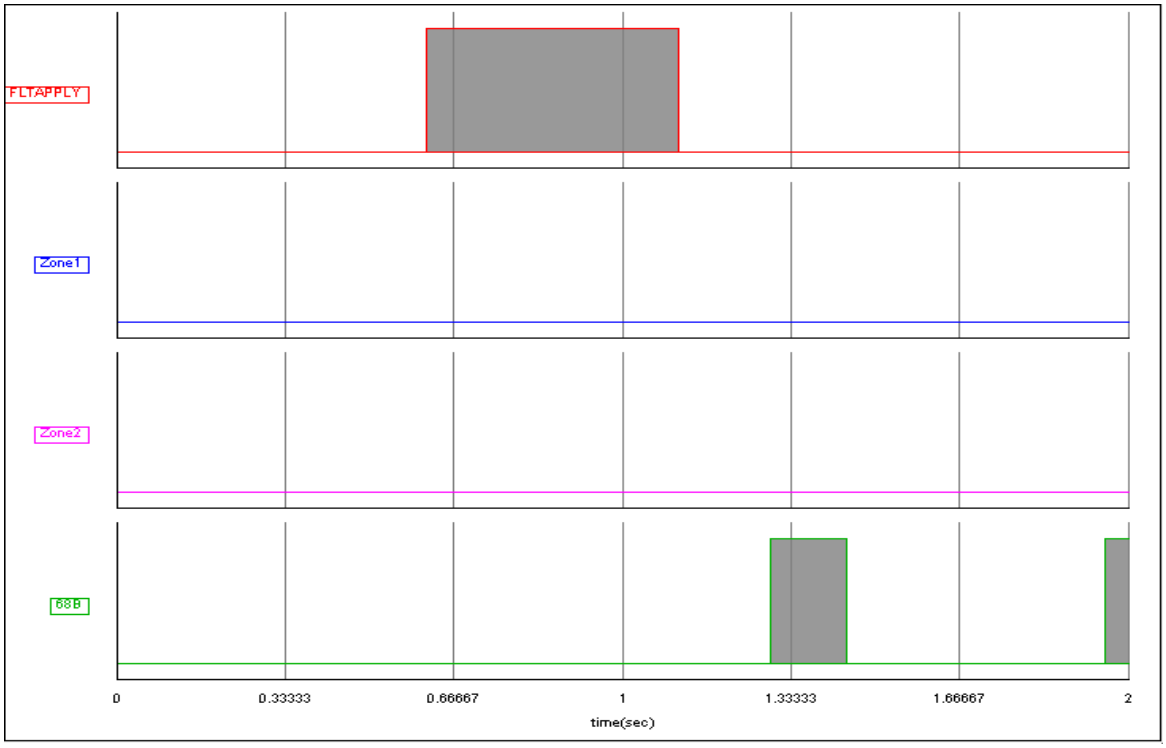

Figure 4.18: Logic Outputs for Fault Detector, Distance Elements and Out of Step Blocking Element- Case A

This event illustrates that original power swing protection settings used with synchronous generators are not adequate for proper detection of OOS with wind generation. Figure 4.17

present the effective impedance response in the positive sequence impedance plane. Figure 4.18 shows the logic outputs for the fault detector, distance protection zone elements and power swing signal detector for this fault.

4.11.2 Case B:Three Phase Fault at Bus 5

In this case a three phase fault is applied at the relay location. We expect the zone 1 instantaneous protection and zone 2 time delayed protection elements to pick up. From the impedance characteristics, it is known that the impedance trajectory enters the zone 1and zone 2 operating characteristics and issues a correct trip signal.

The distance element is at risk of misoperation in this case due to the increased wind generation. This is due to the decrease in overall inertia in the system which produces much faster power swings. The effective positive sequence impedance enters left side inner blinder before detecting the event as fault. This leads to the OST signal being initiated. Therefore, the

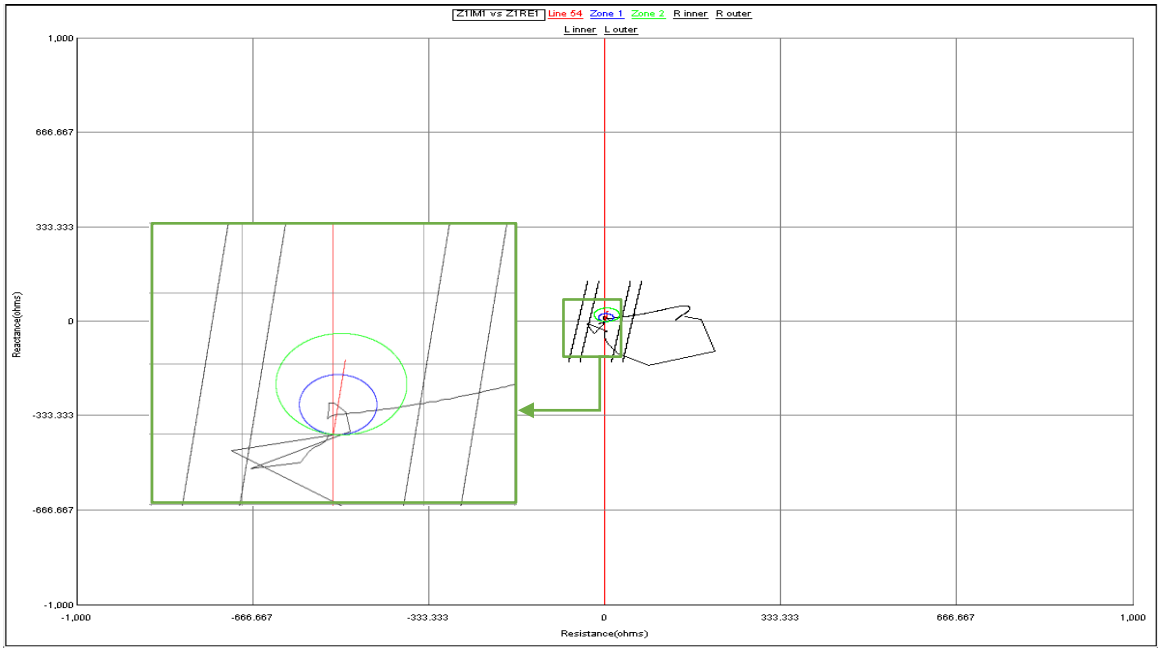

Figure 4.19: Positive Sequence Impedance (Z_1) Plane Plot - Case B

conventional out-of-step protection method cannot be trusted to be reliable with the wind

generation systems. Figure 4.19 gives the details of the impedance trajectory and the Figure 4.20 shows the zone elements of distance protection is being detected for the three phase fault at Bus 5.

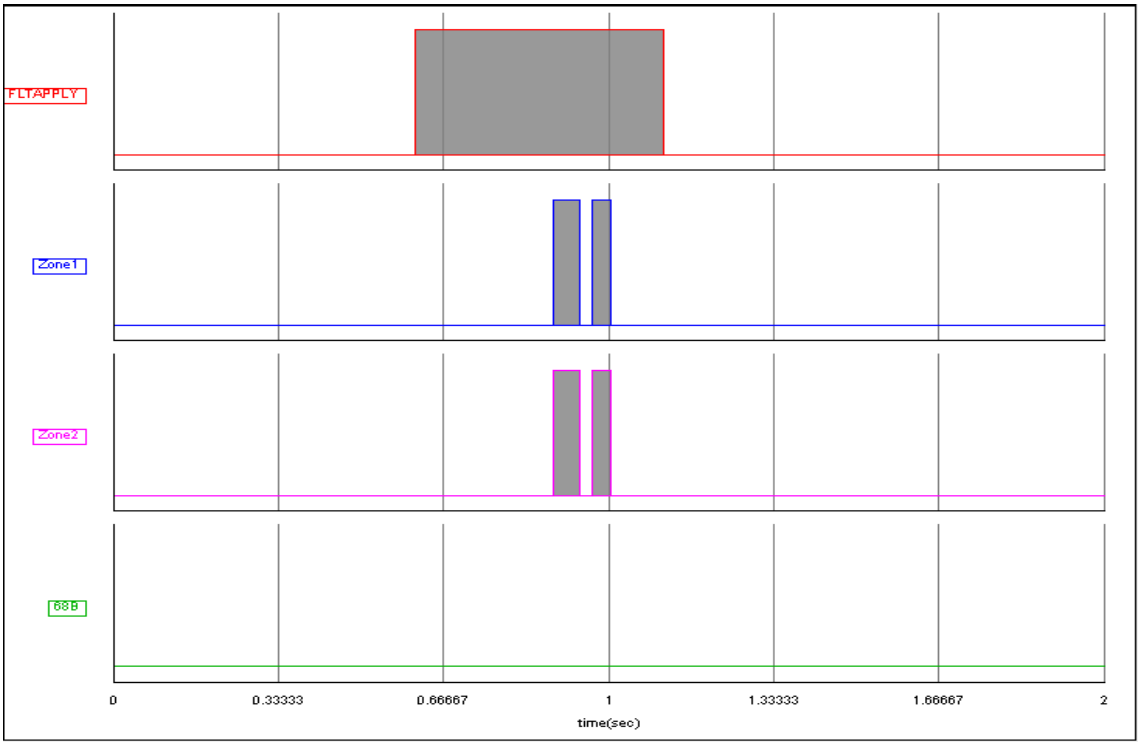

Figure 4.20: Logic Outputs for Fault Detector, Distance Elements and Out of Step Blocking Element- Case B

4.11.3 Case C: Unbalanced LLG (BCG) Fault at Bus 3

When this fault was simulated with only synchronous generators, PSB element blocked the Zone 2 element from pick up for a stable power swing. But when BCG fault is applied at Bus 3 with 200MW of wind generation, the impedance trajectory crosses the right side blinders faster than the PSB time delay setting. Therefore, the power swing protection (68B) fails to detect the power swing and does not issue PSB signal.

Without the swing being detected, the impedance enters in to the zone 2 operating charcteristics of the distance relay and the zone 2 element picks up. If the effective impedance stays in zone 2 long enough for the timer to expire, a trip command will be executed.

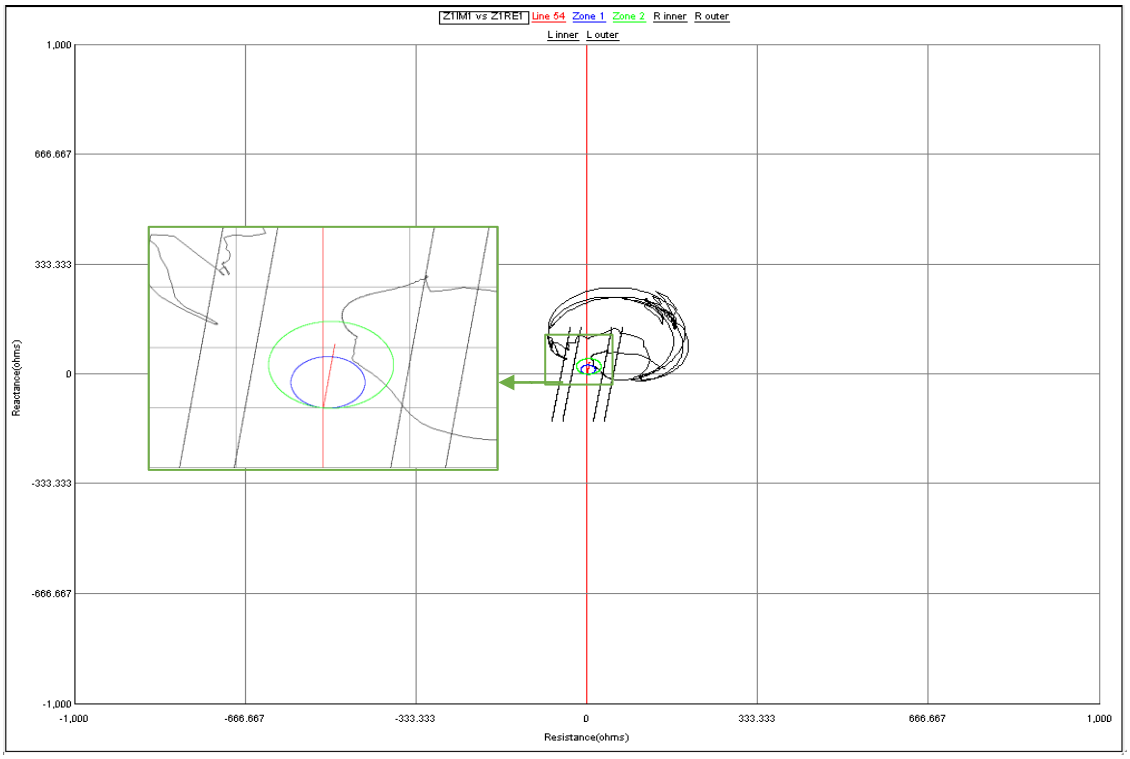

Figure 4.21: Positive Sequence Impedance (Z_1) Plane Plot - Case C

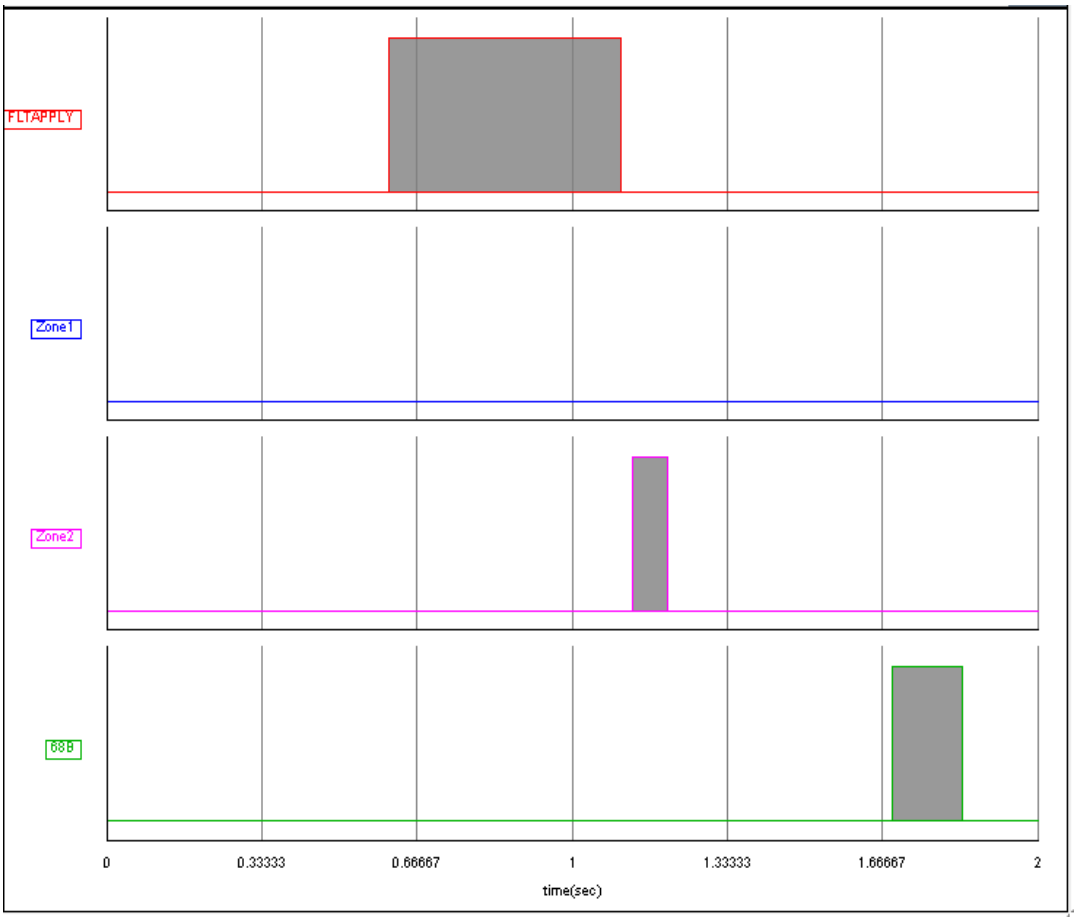

Figure 4.22: Logic Outputs for Fault Detector, Distance Elements and Out of Step Blocking Element- Case C

4.12 Conclusion

The wind power integration system design is demonstrated and simulated in this chapter. The fault simulation cases depict that rate the change of impedance with wind generation increased compared with the synchronous generators in the system with the cases from Chapter 3. The conventional out-of-step protection methods may misoperate and can increase the system unstability during the response to disturbances. Therefore, new methods to differentialte between faults andpower swings for systems with high penetration of inverter based generation.

4.13 Summary

This chapter showed the development of the Type 4 WTG average model for studying its impact on the distance protection element. The performance difference between the WTG and the synchronous generator during the faults in the system is also studied. The distance protection element is found to be affected by the integrated WTG's.

Chapter 5: Proposed Protection Scheme

5.1 Introduction

The results in Chapter 4 showed that the commonly applied out of step blocking elements are not reliable for detecting the power swings in the power system with the integration of a large amount of Type 4 WTG systems. The Park's transformation was applied in Chapter 4 for the implementation of three-phase controls for the power converters. The transformation gives a two-axis rotating reference frame with quantities rotating synchronously with the system frequency. A power swing analysis tool based on Park's transformation is applied using the relay input voltages, where the three-phase quantities are mapped to direct axis and quadrature axis in the synchronous reference frame. Based on the response of the system to disturbances, these quantities are used to determine if a power swings is stable or unstable.

5.2 New Protection Scheme

The voltage at the relay location varies during system disturbances caused by faults, load changes or generator switching. Once a fault occurs in the system, the magnitude of the voltage varies until the breaker is opened to clear the fault. The Park's transformation applied to the relay input voltages according to equation (4.10) implemented in RSCAD as shown in Figure 5.1. The transformed voltage amplitudes are analyzed to detect the fault and power swings with wind integrated systems.

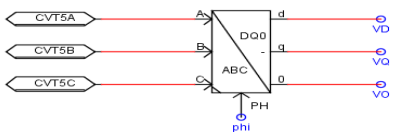

Figure 5.1: Parks Transformation Applied to the CVT voltages

The direct axis (V_D) and quadrature axis (V_Q) voltage waveforms under the steady-state operation of the wind integrated system are shown in Figure 5.2.

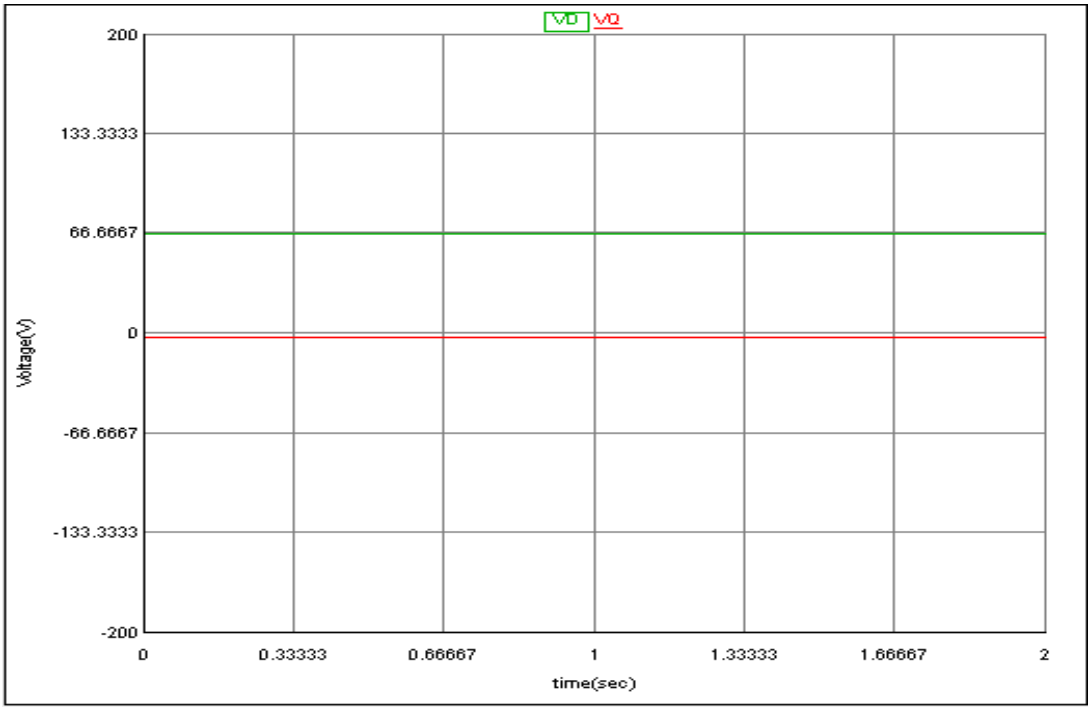

Figure 5.2: Direct Axis (V_D) and Quadrature Axis (V_Q) Relay Voltage Waveforms

The voltage input to the relay varies when there is a disturbance in the system. The direct axis voltage magnitude can be used to classify disturbances such as faults or power swings and protective measures can be taken in response to power swings by issuing a trip signal or blocking the signal.

In a typical microprocessor relay, the output values of the voltage transformer are fed to a loop with an anti-aliasing filter, A/D converter and a Fourier filter for calculating phasor magnitude and angle. In this thesis, we are analyzing system disturbances using a build-in protective relay model available in RSCAD. The simulation responses for the direct axis voltages are processed through a low-pass band filter with a cut-off frequency of 30 Hz.

5.3 Simulation Results

5.3.1 Case A: Three-phase fault at Bus 4

In this case a three-phase fault occurs at Bus 4, which is at 100% of the line relative to the relay location at Bus 5. The voltage seen by the relay changes and the direct axis voltage V_D also changes. The value of V_D drops to nearly half of the rated value with the inception of the fault and remains constant until the fault is cleared. Immediately after the fault is cleared, the V_D returns to its steady-state operating point following some system oscillation with a small deviation from the rated value. Figure 5.3 shows the variation of the V_D with respect to the fault applied.

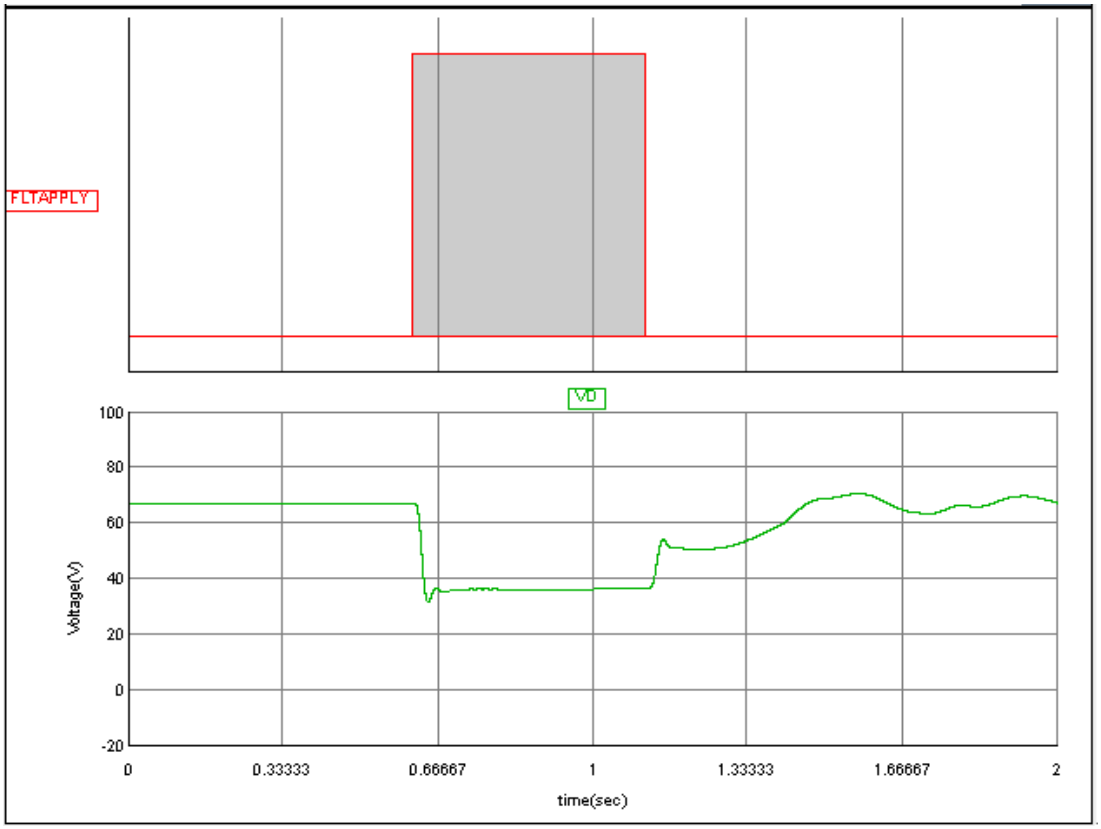

Figure 5.3: Fault Application Signal and Direct Axis Voltage (V_D) for Case A: Three Phase Fault at Bus 4

5.3.2 Case B: Three-Phase Fault at Bus 5

When the three-phase fault occurs at Bus 5, which is at the distance relay location, the voltage drops to zero and remains at a constant value until the fault is cleared. Figure 5.4 shows us the fault applied signal and direct axis voltage, (V_D), where V_D goes to zero and shows a power swing when the system recovers.

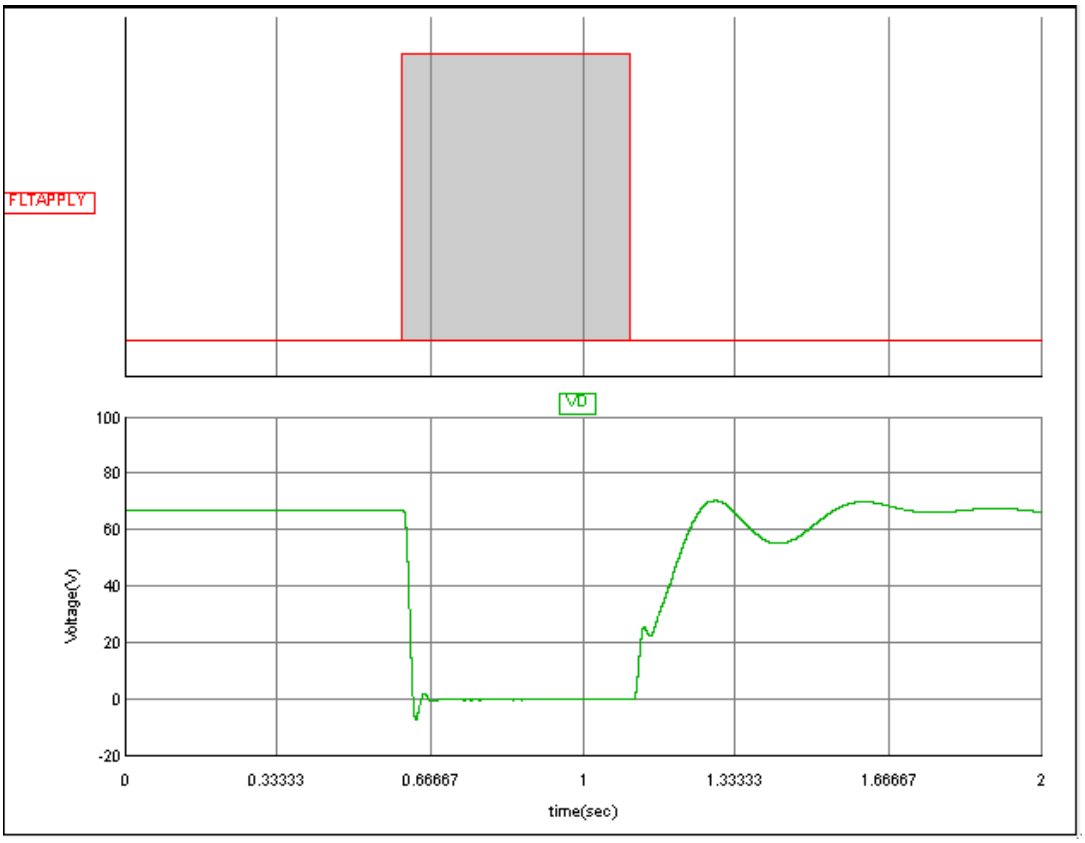

Figure 5.4: Fault Application Signal and Direct Axis Voltage (V_D) for Case B: Three Phase Fault at Bus 5

5.3.3 Case C: Unbalanced LLG (BCG) fault at Bus 3

As a result of the unbalanced LLG fault at Bus 3, V_D gradually decreases until the fault is cleared. After the fault is cleard, V_D starts to gradually increase towards the steady-state value

and oscillates in low frequencies. The correct response of this event is a stable power swing from Figure 3.17, but due to the integration of Type 4 WTG to the 12-bus system, this event resulted in false operation of zone 2 distance element in Figure 4.22 This is because of the increased rate of change of swing impedance causing PSB misoperation.

By using the new protection scheme discussed in Section 5.2, the distance element responds correctly. Figure 5.5 shows the magnitude of the voltage during a power swing along with the fault-initiated signal. If there is a step change in the value of V_D with futher decreasing the value until the fault is cleared, then it is declared as a power swing.

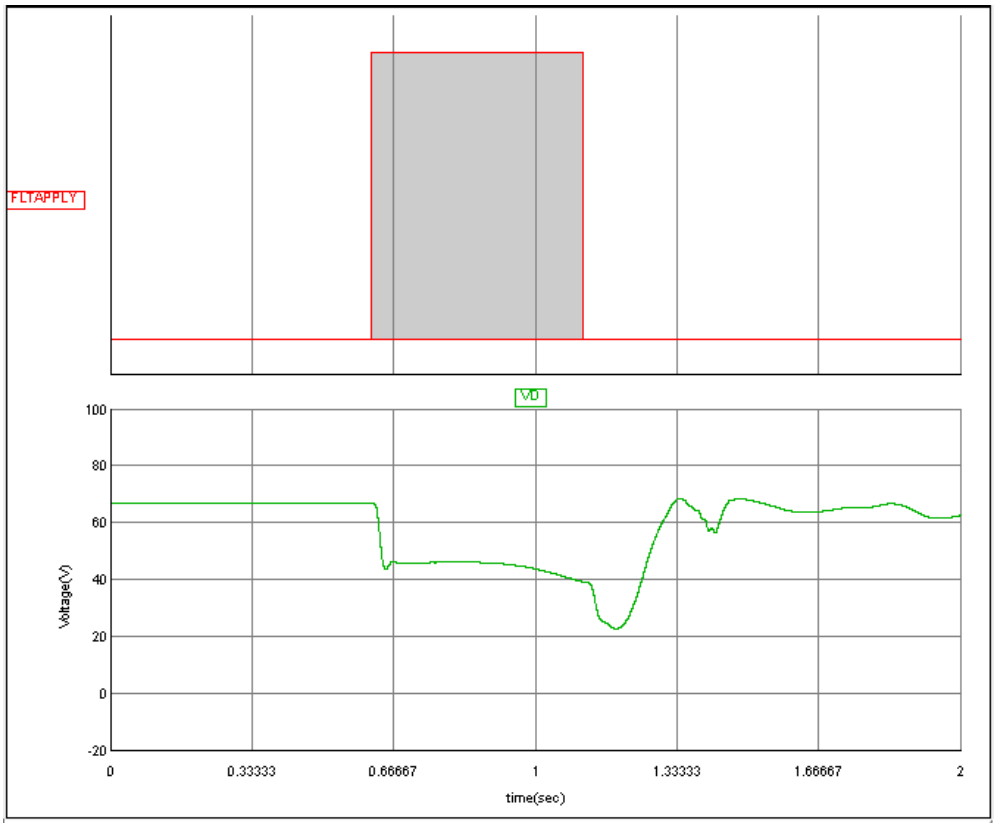

Figure 5.5: Fault Applied Signal and Direct Axis Voltage (V_D) for Case C

However, in order to test the application for differentiating between stable and unstable swing, simulation of an unstable power swing is necessary, without any changes in the element settings other than the new detector.

5.3.4 Case D: Three-phase fault at Bus 2

A 0.5 s three phase fault is initiated at Bus 2 with wind generation, results in the variation of the system voltage and currents.

Figure 5.6 shows the positive sequence impedance plane plot for this case. The impedance trajectory enters the right-side blinders and leaves left-side blinders and the power system cannot regain stability. After the fault is cleared V_D, oscillates between the rated value and zero. This phenomenon is taken into the account and it can be used to detect unstable power swings.

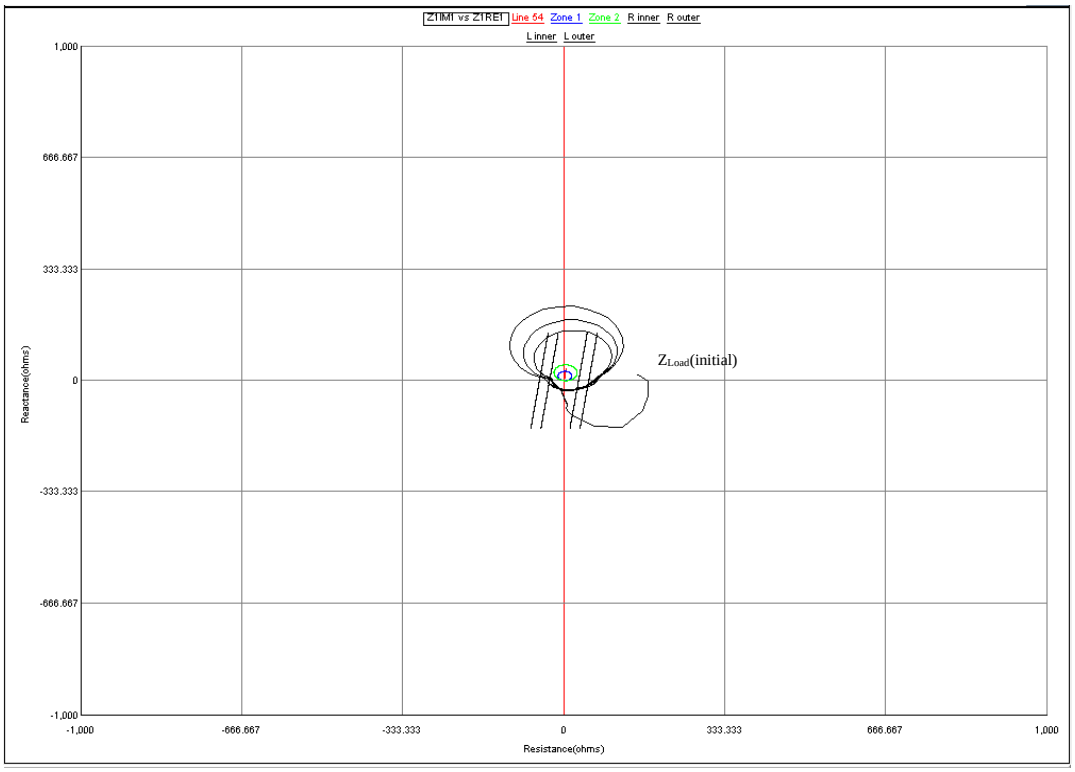

Figure 5.6: Positive Sequence Impedance (Z_1) Plane Plot - Case D

Similar to the stable power swing, the direct axis voltage V_D approaches to its rated value immediately after fault is cleared, however it then oscillates and does not go back to near constant amplitude.

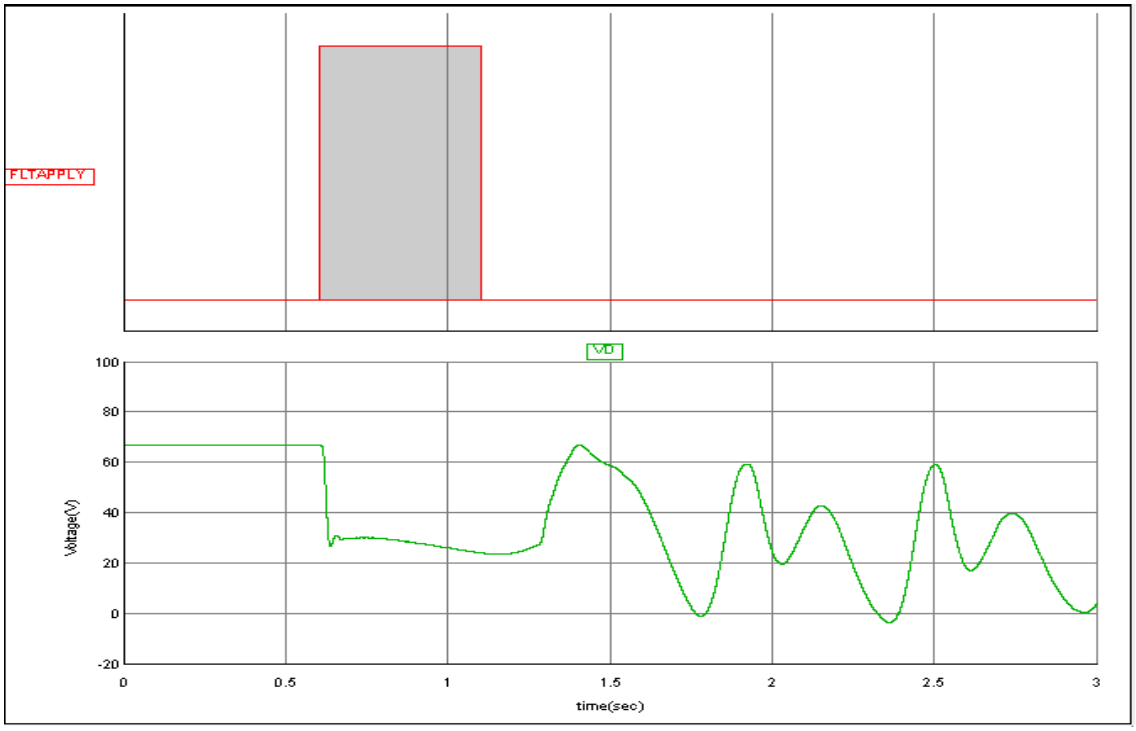

Figure 5.7: Fault Applied Signal and Direct Axis Voltage (V_D) for Case D

5.4 Summary

In this chapter, the basic concepts for new scheme for differentiating power swings from faults for systems with high penetration of Type 4 Wind integrated generation systems was proposed and tested using time domain fault simulations. From the analysis of the fault simulation cases discussed above, this scheme works for wind integrated systems without causing any mis-operation of the distance relay for the cases studied.

Chapter 6 - Conclusions and Future Work

6.1 Conclusion

The power system simulated in this research study gives a good understanding of system dynamic response with high penetration of distributed generation offsetting convention generation and how that impacts power swing detection schemes in distance relays. The response with the aggregated WTG model gives good insight into change in performance of distance protection schemes during power swings between cases with convention generation with large-scale integration of WTGs. The controls of the voltage sourced converter of WTG are change the fault response significantly from the operating characteristics of conventional generators. The impact of wind generation on the power swing protection scheme was investigated. The fault simulated at different bus locations across the system gave a good understanding of the effects on distance protection element power swing blocking and out of step tripping response.

The discussion in Chapter 4 shows that conventional power swing detection schemes designed around synchronous generator dominated systems are not fast enough to inverter based generation dominated systems. . The results presented in the Chapter 4 showed that the relay mis-operates and issues incorrect trip signals for a power swing.

A new out of step protection scheme was proposed based on the variation of the direct axis voltage from Park's transformation to the synchronous reference frame to differentiate faults and power swings for the systems with high penetrations of inverter-based generation. Successful performance of the scheme was demonstrated through different fault simulation cases.

6.2 Future Work

With the response of the system to faults, a new protection scheme for identifying power swings was proposed and demonstrated. Based on the observation and analysis, the following topics need further study.

1) The simulation results were evaluated using the build-in relay model in RSCAD. This work can be enhanced by using a commercial relay to understand real-time performance of the out of step protection element.
2) Using the converter controls designed in this study, the averaged converter model can be replaced by switching model to determine if any aspects of the switching behavior impact the response of the proposed element.
3) The stability of the power system is reduced because the inertia of Type 4 WTG is nearly zero since the converter tracks system phase angle and frequency variations with a fast time constant to maintain maximum power transfer. The concept of synthetic inertia has been proposed to temporarily extract the rotational energy stored in the wind turbine as active power during power system disturbances can be developed using additional control functions. The impact synthetic inertia response of power swing protection needs to be evaluated.
4) The considered Type 4 WTG topology uses a controlled dc voltage source and dc/ac grid side converter. To study the effects of different wind speed conditions, including rapid wind speed variations, on the power swing protection element a Type 4 WTG model representing a permanent magnet synchronous generator and ac/dc converter interface to the dc bus can be implemented.

5) Additional protection scheme such as differential protection, overcurrent protection, communication-aided protection can be developed in RSCAD. Similar to distance elements, overcurrent elements can mis-operate during fast power swing rates if the current crosses the threshold settings. The performance of communication aided protection scheme during fast power swings should be evaluated.
6) Some wind farms may have different types of wind energy systems, such as combinations of type 2, type 3 and type 4 turbines. The contribution of inertia to the power system grid is different in each type based on the WTG electrical composition. Therefore, studies can be carried out with different types in RSCAD to better understand the effectiveness of traditional power swing protection scheme and check the feasibility of new power swing protection discussed in this thesis.

References

[1] Pieter Tielens, Dirk Van Hertem, “The relevance of inertia in power systems,” *Renewable and Sustainable Energy Reviews*. vol. 55, March 2016, Pages 999-1009.

[2] E. Spahic, D. Varma, G. Beck, G. Kuhn, and V. Hild, "Impact of reduced system inertia on stable power system operation and an overview of possible solutions," in *Proc. PESGM*. Boston, MA, USA, 17–21 Jul. 2016.

[3] IEEE Power System Relaying Committee WG D6, *Power Swing and Out-of-Step Considerations on Transmission Lines*. July 2005. Available: http://www.pes-psrc.org.

[4] A. Haddadi, I. Kocar, U. Karaagac, H. Gras, and E. Farantatos, ‘‘Impact of wind generation on power swing protection,’’ *IEEE Trans. Power Del.* vol. 34, no. 3, pp. 1118–1128, Jun. 2019.

[5] D.A. Tziouvaras, Daqing Hou, "Out-of-step protection fundamentals and advancements," in *57th Annual Conference for Protective Relay Engineers*. pp.282-307, 1 April 2004.

[6] J. Mooney, and N. Fischer, "Application Guidelines for Power Swing Detection on Transmission Systems," *Power Systems Conference: Advanced Metering, Protection, Control, Communication, and Distributed Resources*. 2006. PS '06, pp.159 – 168, March 2006.

[7] F. Ilar, "Innovations in the Detection of Power Swings in Electrical Networks," *Brown Boveri Review*. vol. 2-81, pp. 87-93, 1981.

[8] RTDS technologies. *Real-time digital simulator controls library manual*. July 2013.

[9] J. L. Blackburn and T. J. Domin, *Protective Relaying: Principles and Applications, 3rd Edition*. Boca Raton: Taylor & Francis Group, LLC, 2007.

[10] Ankita Roy, *Protection performance study of a type IV wind turbine system*. Master's Thesis, Dept of Electrical and Computer Engineering, University of Idaho, December 2013.

[11] Amirnaser Yazdani and Reza Iravani: *Voltage-Sourced Converters in Power Systems - Modeling, Control, and Application*s. Wiley, March 2010.

[12] Shan Jiang, U. D. Annakkage, A. M. Gole, "A Platform for Validation of FACTS Models", IEEE Transactions on Power Delivery, Vol. 21, No.1, January 2006.

Appendix A

This appendix shows the calculation of the per unit base values for the system parameters shown in Chapter 3 for calculating the protection element settings.

System Parameters

Resistance of the Line 5-4 (R_{54pu})=0.03356

Reactance of the Line 5-4 (X_{54pu})==0.26656

S_{Base} = 100MVA V_{LL}= 230kV $Z_{Base} = \frac{V_{LL}^2}{S_{Base}}$ = 529 Ohms

$Z_{54L} = (R_{54pu} + jX_{54pu})Z_{Base}$= (17.753+j141.01) Ohms

The equivalent Source Impedance Z_{5S}=(21.605+j73.039) Ohms

The equivalent Source Impedance Z_{5R}=(4.156+j17.048) Ohms

The Total Transfer Impedance $Z_T = Z_{5S} + Z_{54L} + Z_{5R}$

CT calculations:

I_{Base} = 434.783A

Maximum fault current at Bus 5 $I_{maxFault} = 2.174$kA

$$CTR = \frac{2.5\text{kA}}{5\text{A}} = 500$$

CVT calculations:

Secondary Voltage of the CVT transformer= 115V

$$\text{PTR} = \frac{230\text{kV}}{115\text{V}} = 2000$$

Determination of Distance Element Settings

Secondary Impedance $\text{Z}_{\text{Sec}\,54} = \text{Z}_{54\text{L}}\frac{\text{CTR}}{\text{PTR}}$ = (4.438+j35.253) ohms

Secondary Total Transfer Impedance $\text{Z}_{\text{SecT}} = \text{Z}_{\text{T}}\frac{\text{CTR}}{\text{PTR}}$ = (10.878+j57.774) ohms

$|Z_{Sec\,54}|$=35.531 ohms

Zone 1 = 80%$|Z_{Sec\,54}|$ =28.425 ohms Zone 2 = 135%$|Z_{Sec\,54}|$= 47.967 ohms

Determining Inner Resistive Blinders

Inner Angle = δ_1 = 90Degree

Inner Blinder Setting = $\frac{|Z_{SecT}|}{2\tan\left(\frac{\delta_1}{2}\right)}$ = 29.395 ohms

Determining Outer Resistive Blinders

Outer Angle = δ_2 = 60Degree

Outer1 Blinder Setting = $\frac{|Z_{SecT}|}{2\tan\left(\frac{\delta_2}{2}\right)}$ = 50.913 ohms

Determining Power Swing Blocking Delay

Slip frequency =s= 5 Hz

Blocking Delay = $\frac{(\delta_1 - \delta_2)*60\text{Hz}}{\text{s}*360\text{Deg}}$ = 1cycle

Power Swing Blocking Delay in sec = 16.667ms

Appendix B

This appendix shows the calculations of system parameters used in Chapter 4

22kV Type 4 WTG system

Rated Active Power $P_w = 510\text{MW}$

Rated Reactive Power $Q_w = 9\text{MVAr}$

Rated Voltage $V_{LL} = 22\text{kV}$

$S_{BaseW} = 550\text{MVA}$

$$Z_{BaseW} = \frac{V_{LL}^2}{S_{BaseW}} = 0.88 \text{ ohms}$$

The reactance between the VSC terminals and Bus 11 = L= 0.35mH

The resistance between the VSC terminals and Bus 11 = R=6.6 mΩ

Transformer

The transformer for a Type 4 WTG will generally be a Delta-Star ground transformer. The rating of the transformer is given below

Primary Voltage V_P =22kV

Secondary Voltage V_s = 230kV

Transformer MVA =800MVA

Leakage Reactance = 0.065pu